EvoIR-Agent: Self-Evolving Image Restoration Agentic System via Experience-Driven Learning

Kailin Zhuang, Jiawei Wu, Zhi Jin*
School of Intelligent Systems Engineering
Shenzhen Campus of Sun Yat-sen University, Guangdong, China
zhuangklin@mail.sysu.edu.cn

Abstract

Multimodal Large Language Model (MLLM)-driven image restoration agent demonstrates effectiveness in degradation coupling scenarios by flexibly selecting tools and determining removal orders. However, their zero-shot planning often fails without experience, necessitating severe trial-and-error overhead to achieve satisfactory outcomes. Currently, two paradigms are employed to address this issue, yet a dilemma persists: Training-based methods embed intrinsic experience into parameters, achieving high inference efficiency but lacking compatibility with new tools or degradation. In contrast, training-free methods utilize explicit experience storage for compatibility but still incur trial-and-error overhead due to naive experience. To resolve the dilemma, we propose **EvoIR-Agent**, which first systematically formulates the experience components of a training-free image restoration agent. Subsequently, a hierarchical experience pool is constructed, which enables coarse-to-fine guidance for diverse tools and removal orders. Furthermore, a self-evolving mechanism is introduced to update the pool from scratch using accumulated records, thereby greatly improving performance and efficiency. Extensive experiments reveal that **EvoIR-Agent** achieves a significant lead in the full reference metrics and yields a remarkable Pareto-optimal balance between performance and efficiency compared to the state-of-the-art methods. Our codes are available at https://github.com/rightleft-123/EvoIRAgent

1 Introduction

Image restoration (IR) is a low-level vision task that aims to recover a high-quality (HQ) image from a degraded low-quality (LQ) version. In recent decades, considerable progress has been made in addressing IR problems related to specific tasks [1, 2, 3, 4, 5]. However, in real-world scenarios, multiple degradations are often coupled, making restoration more challenging.

A promising direction for addressing this challenge is all-in-one image restoration (AiOIR), which aims to handle multiple degradations with a unified model [6]. The majority of methods [7, 8, 9, 10, 11, 12] aim to address the degradation coupling problem by learning more general degradation feature representations. While significant strides have been made, they are still limited to a few types of degradation and are difficult to extend to new degradations without retraining.

Recent advances in Multimodal Large Language Models (MLLMs) [13, 14] have inspired a new direction in IR, namely Image Restoration Agent (IRA). The key is to leverage a MLLM-driven agent to select restoration tools and determine removal orders. However, general-purpose MLLMs encounter difficulties with zero-shot planning [15, 16] without experience-driven, which results in severe trial-and-error overhead to reach satisfied restoration result. To resolve this issue, existing methods can be divided into two distinct paradigms. Training-based methods [15, 17, 18] internalize intrinsic experience into model parameters, offering high inference efficiency but lacking compatibility for new tools or degradation. Conversely, training-free methods [16, 19, 20] utilize external containers for

*Corresponding author. Also with Guangdong Provincial Key Laboratory of Fire Science and Intelligent Emergency Technology, Shenzhen, China.

Preprint.

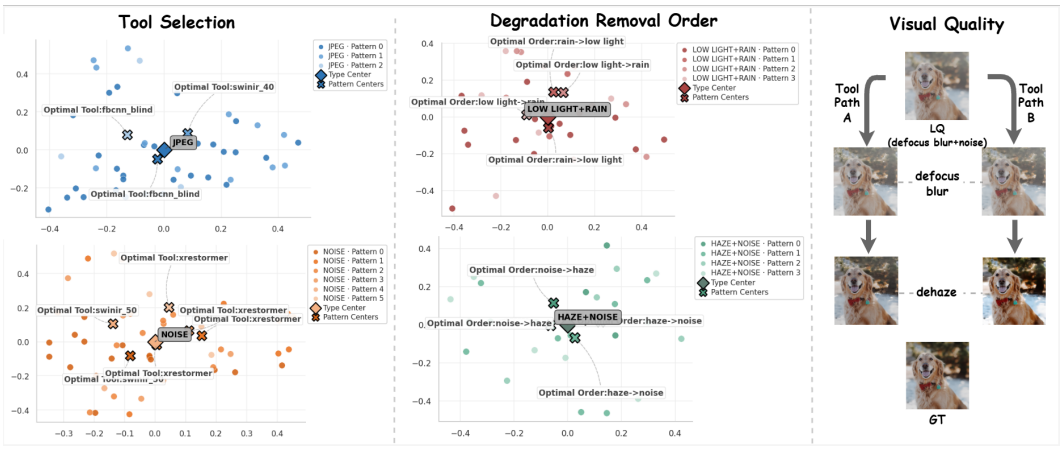

Figure 1: Illustration of the experience components in IRA. (Left&Center) We extract embeddings of various degraded images using an image encoder [25]. The scatter plots reveal that images sharing a degradation type may cluster into different degradation patterns. Crucially, the optimal *Tool Selection* and *Degradation Removal Order* are highly pattern-dependent. (Right) *Visual Quality* demonstrates that divergent tool paths can successfully achieve restoration but yield distinct visual quality.

explicit experience storage, while highly compatible, they still result in considerable trial-and-error overhead owing to being guided by naive experience. Therefore, we aim to retain the compatibility of training-free methods while endowing the model with the inference efficiency of training-based methods. We identify that the considerable trial-and-error overhead in training-free IRAs stems from the underdeveloped experience mechanism. To systematically break this bottleneck, we revisit from two perspectives: (i) *Do existing IRAs lack an experience mechanism altogether?* Not entirely. Recent frameworks [16, 19, 20] already incorporated experience mechanism. However, their experience components remain simplistic and static, preventing the agent from accepting comprehensive and dynamic guidance. (ii) *Is it possible to transfer well-established experience mechanisms from general-purpose agents to IRAs?* It is possible. Recent advancements [21, 22, 23, 24] have demonstrated that explicit experience drives self-evolving skills in general-purpose agents. However, it is unrealistic to directly apply to IRAs without a domain-specific redesign.

Thereby, we introduce **EvoIR-Agent**, an image restoration agentic system explicitly designed to address the domain-specific needs. We first clearly identify the experience components in IRA as illustrated in Figure 1. (1) *Tool Selection*: The optimal tool depends not merely on broad degradation type, but on specific degradation pattern [15]. Experience is designed to explicitly map these patterns to their optimal tool; (2) *Degradation Removal Order*: Similarly, in degradation coupling settings, the optimal order is also pattern-dependent; (3) *Visual Quality*: Due to inherent attributes in different tools, multiple paths may address the degradation, but result in significantly different visual outcomes. Overall, current experience mechanism focuses on removal order, with a few addresses on tool selection and showing an absence in focusing on visual quality. Moreover, they concentrate on the broad degradation type, while neglecting to delve into the degradation pattern at a finer granularity.

To systematically capture this coarse-to-fine information in conjunction with the aforementioned three experience components, we feature a hierarchical experience pool for storage. Inspired by [26, 27, 28], this pool retrieves contextually relevant experience across multiple levels, providing the IRA with robust, prioritized experience guidance. Building upon this structural foundation, the pool is equipped with a self-evolving experience mechanism. Unlike prior static experiences, ours iteratively updates its experience pool using newly accumulated records. This dynamic evolution enables the system to adapt to tools and degradation on the data source, thereby promoting performance and inference efficiency. Our main contributions are summarized as follows:

(1) Systematic Formulation. We reformulate the experience components in IRAs by introducing *visual quality* as an additional component. We also identify a limitation in current IRA experience: a singular focus on broad degradation types, with an absence of finer degradation patterns.

(2) Self-Evolving Architecture. To effectively manage the formulated experience, we propose a hierarchical experience pool equipped with tailored retrieval methods. Building upon this structure, we introduce a self-evolving experience mechanism that updates the pool using accumulated records.

(3) Empirical Evaluation. Extensive experiments demonstrate that **EvoIR-Agent** achieves a superior performance-efficiency trade-off compared to state-of-the-art methods. Furthermore, the results validate the profound impact of the experience mechanism and its capacity for self-evolving.

2 Related Work

All-in-one Image Restoration. All-in-one image restoration aims to handle multiple degradations within a unified model [6]. AirNet [7], and MiOIR [29] focus on designing a unified backbone to model diverse degradation distributions. PromptIR [30] uses learnable prompts to modulate the network for different degradations. DA-CLIP [31] exploits degradation-aware vision-language priors, and InstructIR [9] extends this idea by using human instructions for more flexible restoration control. Some methods leverage generative priors to enhance restoration quality. AutoDIR [10], UniRestore [32], and Defusion [33] formulate restoration in a diffusion framework. Later methods explore richer conditioning or more general restoration representation [12, 34]. However, these works are constrained to a limited number of degradation types, and their capacity for extension is limited.

Image Restoration Agent. Existing image restoration agent approaches can be broadly divided into training-based and training-free methods. Training-based methods, such as RestoreAgent [15] and Q-Agent [35], equip the MLLM with degradation perception and planning capability through fine-tuning. Restore-R1 [17] follows a related direction by using a powerful MLLM as a weak supervision signal to train a lightweight perception-and-planning model. Recent work TIR-Agent [18] and PaAgent [36] both follow in leveraging reinforcement learning (RL) for efficiency planning. In contrast, training-free methods focus on system design. AgenticIR [16], MAIR [19], and 4KAgent [20] place significant emphasis on agentic workflow orchestration. HybrideAgent [37] emphasizes user interaction by means of a design on fast and slow agents for differing requirements. Nevertheless, these works neglect to incorporate a robust experience mechanism for sustainable learning.

Experience Mechanism in General-Purpose Agent. Recent methods have demonstrated that explicit experience can enhance the agent's capabilities, surpassing the limitations of parametric updates [38, 39]. Early agentic systems, such as ExpeL [21], implement this idea by collecting and reflecting trajectories in natural language, then retrieving distilled information at test time. Subsequent works [40, 41] examine not only how to store experience, but also how to manage it. While ProcMEM [42] and ReMe [43] emphasize procedural memory, converting experiences into reusable skills or dynamically refined action knowledge. Finally, FLEX [44] and SimpleMem [45] treated experience as the engine of continual adaptation. Overall, existing methods suggest that the experience mechanism in agent is evolving from simple episodic replay toward selective memory management, promising the system's ability to evolve and adapt.

3 Methodology

This section introduces the closed-loop framework of the **EvoIR-Agent**. As demonstrated in Figure 2, we begin with the outer loop by establishing the five-process inference workflow (Sec. 3.1). Subsequently, we shift to the inner loop and begin with mathematically formulating the experience. By encapsulating three core components—tool selection, degradation removal order, and visual quality—we model the experience by a priority-driven mapping function p (Sec. 3.2). To manage these components, we design a hierarchical experience pool structured across three granularities. This architecture practically instantiates p specifically for each level, providing coarse-to-fine guidance during inference (Sec. 3.3). Ultimately, we introduce a self-evolving experience mechanism that functions in a batch-wise manner. This mechanism enables the continuous updating of p from accumulated records, thereby ensuring performance-efficiency improvement. (Sec. 3.4).

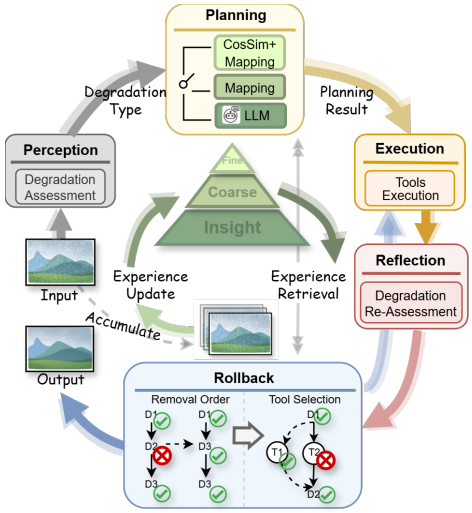

Figure 2: Overview of the experience-driven inference workflow in **EvoIR-Agent**.

3.1 Experience-Driven Inference Workflow

The five-processes inference workflow adopted in prior training-free IRAs [16, 19] is maintained. Formally, given a degraded image I_D, the *Perception* process identifies the degradation types, denoted as $D = \{d_1, d_2, \dots\}$. Based on the result, the *Planning* process performs decision-making with the degradation removal order O, which is defined as a permutation over D, i.e., $O \in \Pi(D)$. Adhering to this plan, the *Execution* process utilities a series of restoration tools for specific degradation d_i defined as $T = \{\tau_{d_1}^1, \tau_{d_1}^2, \dots, \tau_{d_2}^1, \dots\}$ to obtain the restored image $\hat{I}_D$. The *Reflection* process is then performed to evaluate if all D have been effectively eliminated on $\hat{I}_D$. If so, the process terminates and outputs the image. Otherwise, the *Rollback* process is triggered. The utilization of the experience pool enables the MLLM to accept robust guidance during the *Planning* and *Rollback* processes, and facilitates the management of O and T usage. Specifically, during rollback, O is revised first, followed by the refinement of T to preserve the integrity of the experience guidance.

3.2 Experience Formulation

We first define the aforementioned concept of visual quality. Observations from the restored images $\hat{I}_D$ from prior works (detailed in Appendix A.1) reveal a critical phenomenon: distinct tool selections can yield the restored images that exhibit divergent visual quality. We conceptualize these differences as a *Preference* requirement, denoted by Q. It signifies a subjective preference interpretation that can be specified by humans and supported by different image quality assessment (IQA) metrics. In this work, *Fidelity* and *Perception* are specified as *Preference* requirements.

Subsequently, we mathematically formulate the guidance provided by the experience as a priority-driven mapping function p. The objective of *Tool Selection* is:

$$\tau^* = p\big(T(d) \mid Q, d, H\big), \tag{1}$$

where $T(d) \subseteq T$ indicates the candidate tool set corresponds to a degradation type d, and H contains the historical information during the decision-making process in the inference stage.

In cases of greater complexity with degradation coupling setting, the objective of determining the *Degradation Removal Order*, denoted by O, should be established in conjunction with the relevant restoration tools $T(D)$ according to priority p:

$$o^* = p\big(O \mid Q, T(D), D, H\big). \tag{2}$$

Experience Foundation. As illustrated in the left panel of Figure 3, it should be noted that the number of permutations in O increases exponentially as D and T rise. This makes direct experience modeling inefficient and redundant. Therefore, we propose to simplify the condition on experience and form as a foundation. The details are provided in the Appendix A.1. Here's a summary:

- Considering restoration in degradation coupling settings, when specifying the preference Q, the optimal tool τ^* will be utilized to explore the degradation removal order O. This process will reduce the joint optimization from $\prod_{d_i \in D} \mathcal{T}(d_i)$ search space down to a purely D-centric permutation problem in preference requirement Q.

3.3 Hierarchical Experience Pool

In light of the aforementioned formulation and the findings presented in Figure 1, the optimal τ^* and o^* depend not only on the degradation type but also on the degradation pattern. Therefore, we draw inspiration from the hierarchical experience pool used in general-purpose agents, which effectively balances information across different granularities. Adopting this structure leads to a distinct instantiation of the priority-driven mapping function p:

Insight Level (Preference-oriented): At the highest level, p is instantiated by a LLM. For given Q and D, the LLM leverages distilled textual experience to guide the planning on o.

Coarse-grained Level (Degradation Type-oriented): This level instantiates p into a direct key-value mapping without the MLLM involved. Utilizing Q and D as the query, the value is considered as o.

Fine-grained Level (Degradation Pattern-oriented): According to Figure 1, a degradation type may cluster into different degradation patterns. This level still instantiates p into a key-value mapping,

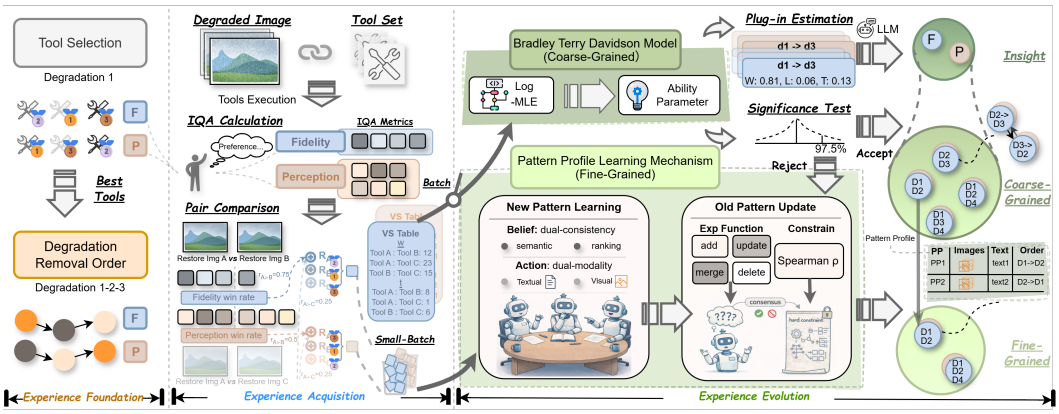

Figure 3: Overview of the inner closed-loop experience mechanism in **EvoIR-Agent**. (Left) Experience pool works as a priority-driven mapping problem. (Middle) Using priority-aware modeling to generate an atomic experience record. (Right) Batch-wise experience evolving mechanism for the hierarchical pool to update the priority function.

while combined with a retrieval strategy. The core intuition here is that a similar degradation pattern exhibits a similar priority function p. We first anchor these specific patterns using a *pattern profile*:

$$P = \left(\{I_D^{(i)}\}_{i=1}^{m},\ text \right), \tag{3}$$

where $\{I_D^{(i)}\}$ is a supporting set of degraded images characterizing the pattern, and text is its semantic description. (The construction of P is detailed in Section 3.4). During inference, given an input image I_D along with Q and D, we execute a two-stage cascade retrieval. First, we employ a CLIP encoder $e(\cdot)$ [25] to recall the Top-K relevant profiles based on cosine similarity:

$$\mathrm{CosSim}(P, I_D) = \frac{e(P) \cdot e(I_D)}{|e(P)|\,|e(I_D)|}. \tag{4}$$

Subsequently, the MLLM evaluates the Top-K candidates $text$ against the input image to identify the most accurate profile P^*. Ultimately, P^* is utilized as a query condition, value is considered as o.

In light of the preceding experience foundation, the aforementioned three levels are characterized by the automatic selection of τ on each d with preference Q according to the coarse-grained level.

3.4 Self-Evolving Experience Mechanism

Based on the previous formulation of each experience and the structure of the experience pool, this section explains how the entire self-evolving experience mechanism is applied to the experience pool and operates in generating the latest priority-driven mapping function p.

Experience Acquisition. As illustrated in the middle panel of Figure 3, we undertake an exhaustive exploration of all potential outcomes to establish the comprehensive priority-aware model to generate an atomic experience record, which bootstraps the subsequent evolution stage.

Within an atomic experience record, a degraded image I_D with degradation types D and its corresponding tools $T(D)$ are employed, thereby yielding a set of restoration images:

$$\hat{I}_D = \{\hat{I}_D^1, \ldots, \hat{I}_D^N\},\ \text{where } N = \begin{cases} |T(D)|, & |D| = 1 \\ |D|!, & |D| > 1 \end{cases} \tag{5}$$

Subsequently, the results are evaluated using IQA metrics according to preference Q. A pairwise comparison is performed on each metric in regard to the restoration images $\hat{I}_D$:

$$r_{i \succ j} = \frac{1}{|M|} \sum_{m \in M} \mathbb{I}_m(i \succ j), \quad \mathbb{I}_m(i \succ j) = \begin{cases} 1, & m \in M\uparrow \text{ and } m(\hat{I}_D^i) > m(\hat{I}_D^j) \\ 1, & m \in M\downarrow \text{ and } m(\hat{I}_D^i) < m(\hat{I}_D^j), \\ 0, & \text{otherwise} \end{cases} \tag{6}$$

where $M\uparrow$ and $M\downarrow$ denote the higher-is-better and lower-is-better metrics, respectively. Based on these, we derive the win rate pair $r_{i\succ j}$ along with the win/loss/tie statistics w_{ij}, l_{ij}, and t_{ij}, where $r_{i\succ j} > 0.5$ indicates a vote for i, $r_{i\succ j} < 0.5$ indicates a vote for j, otherwise, considered a tie.

Following this, the average win rate of each tool is calculated, and its ranking is derived via sorting:

$$R_i = \frac{1}{|\hat{I}_D| - 1} \sum_{j \neq i} r_{i\succ j}, \qquad \text{rank}_i = \text{rank}_{\downarrow}(R_i). \tag{7}$$

Experience Evolution. As illustrated in the right panel of Figure 3, once a set of B atomic experience records has been collected for D, the process will be triggered on the batch. Ultimately, the designated level of D will be used in inference.

In the coarse-grained level, the self-evolving process commences with the utilization of the latest win/loss/tie counts w_{ij}, l_{ij}, and t_{ij} in B rounds in conjunction with the preceding counts. Leveraging these statistics, the ***Bradley–Terry–Davidson (BTD)*** model [46] is adopted for the purpose of parameterizing the win/loss/tie relations in a probabilistic manner:

$$P(i \succ j) = \frac{e^{\theta_i}}{e^{\theta_i} + e^{\theta_j} + 2\nu e^{(\theta_i+\theta_j)/2}}, \quad P(i = j) = \frac{2\nu e^{(\theta_i+\theta_j)/2}}{e^{\theta_i} + e^{\theta_j} + 2\nu e^{(\theta_i+\theta_j)/2}}, \tag{8}$$

where $\nu \geq 0$ denotes the tie-intensity parameter, and θ defines as the ability parameter. θ can be estimated by maximizing the log-likelihood through a numerical process. Subsequently, θ is sorted and can be regarded as the latest priority function p in coarse-grained granularity:

$$p = \text{argsort}(\hat{\theta}), \qquad \hat{\theta}_1 > \hat{\theta}_2 > \cdots > \hat{\theta}_k. \tag{9}$$

We undertake significance testing in θ to ascertain whether fine-grained experience is necessary. A one-sided Wald test [47] is performed on the Top-ranked candidates θ at a significance level of α. The ability gap between two candidates is measured by $\hat{d}_{ij} = \hat{\theta}_i - \hat{\theta}_j$. We regard as significant if:

$$\hat{d}_{ij} - z_\alpha \, SE(\hat{d}_{ij}) \geq 0, \tag{10}$$

where SE denotes the standard error of θ. If the condition is met, no finer experience is demanded. Otherwise, additional fine-grained experience modeling is triggered.

In the insight level, derived from the latest estimated ability parameter θ, the pairwise win/loss/tie relations can be deduced using Equation (8). Following this procedure, the deduced relations are then concatenated into textual form and combined with a guidance prompt. This enables LLM to distill textual experience, and it will be regarded as the latest priority function p in insight granularity:

$$p = \text{LLM}(\text{Guidance}, \text{Concate}(P(i \succ j), P(i = j))) \,. \tag{11}$$

In the fine-grained level, experiences necessitate a focus on the degradation pattern. We align with the previous definition of P, which anchors similar degradation patterns. However, it should be noted that the categories of P are not predefined in advance, and thus require a learning mechanism. A useful P must satisfy the following two requirements:

- **Semantic consistency** C_s: The images $\{I_D^{(i)}\}_{i=1}^m$ in P should be close in the semantic space to form a compact feature, thus facilitating retrieval by image encoder [25].
- **Ranking consistency** C_r: The priority p mapping to P should be statistically comparable. This ensures that the priority p of a similar P in the experience pool can be reused.

In accordance with these, an agent-driven pattern profile learning mechanism is designed to fully leverage the multimodal comprehension capability of the MLLM.

Using cached rank_i in the latest B rounds, the system performs learning in a mini-batch-wise manner. For each degraded image I_D^i in the small batch, we first generate a degradation description desc_i by MLLM. Subsequently, the multi-agent debate (MAD) [48, 49] paradigm is employed to partition the current small batch into a new pattern profile:

$$P_{\text{new}} = \text{MAD}(\text{role}, \text{action}, \mathcal{C}), \quad \mathcal{C} = \{C_s(\text{desc}),\ C_r(\text{rank})\}, \tag{12}$$

where *role* specifies the agent's designated roles included in the system, *action* encapsulates some predefined executable operations with dual-modality, and $\mathcal{C}(\cdot)$ denotes the dual-consistency requirements mentioned above, which are achieved as the belief [50] for each agent.

Table 1: Quantitative comparison under different degradation settings (Groups A–C) in two *Preference* (Fidelity and Perception). We compare methods within two distinct tool settings in accordance with the baseline methods for fair comparison: **Setting I** (AgenticIR-based) and **Setting II** (4KAgent-based). Rankings (**First** , Second , Third) are calculated independently within each group.

Degrad.	Setting	Method	Fidelity			Perception		
			PSNR ↑	SSIM ↑	LPIPS ↓	MANIQA ↑	CLIP-IQA ↑	MUSIQ ↑
Group A	Setting I	AirNet	19.13	0.6019	0.4283	0.2581	0.3930	42.46
		PromptIR	20.06	0.6088	0.4127	0.2633	0.4013	42.62
		MiOIR	20.84	0.6558	0.3715	0.2451	0.3933	47.82
		DA-CLIP	19.58	0.6032	0.4266	0.2418	0.4139	42.51
		InstructIR	18.03	0.5751	0.4429	0.2660	0.3528	45.77
		AutoDIR	19.64	0.6286	0.3967	0.2500	0.3767	47.01
		AgenticIR	21.04	0.6818	0.3148	0.3071	0.4474	56.88
		MAIR	21.02	0.6715	0.2963	0.3330	0.4751	59.19
		EvoIR-Agent-I	**23.49**	**0.7368**	**0.2840**	**0.3440**	**0.4889**	**60.10**
	Setting II	4KAgent	21.48	0.6720	0.3019	0.3748	**0.5544**	63.19
		TIR-Agent	22.07	0.6935	**0.2874**	**0.3907**	0.5454	**63.69**
		EvoIR-Agent-II	**23.86**	**0.7488**	0.3085	0.3623	0.5204	61.82
Group B	Setting I	AirNet	19.31	0.6567	0.3670	0.2882	0.4274	47.88
		PromptIR	20.47	0.6704	0.3370	0.2893	0.4289	48.10
		MiOIR	20.56	0.6905	0.3243	0.2638	0.4330	51.87
		DA-CLIP	18.56	0.5946	0.4405	0.2435	0.4154	43.70
		InstructIR	18.34	0.6235	0.4072	0.3022	0.3790	50.94
		AutoDIR	19.90	0.6643	0.3542	0.2534	0.3986	49.64
		AgenticIR	20.55	0.7009	0.3072	0.3204	0.4648	57.57
		MAIR	20.92	0.7004	0.2788	**0.3544**	**0.5084**	**60.98**
		EvoIR-Agent-I	**23.41**	**0.7589**	**0.2753**	0.3535	0.4984	**60.98**
	Setting II	4KAgent	20.95	0.6727	0.3017	0.3734	**0.5505**	62.69
		TIR-Agent	22.80	0.7340	**0.2725**	**0.3997**	0.5488	**65.24**
		EvoIR-Agent-II	**23.38**	**0.7643**	0.3117	0.3735	0.5296	61.96
Group C	Setting I	AirNet	17.95	0.5145	0.5782	0.1854	0.3113	30.12
		PromptIR	18.51	0.5166	0.5756	0.1906	0.3104	29.71
		MiOIR	15.63	0.4896	0.5376	0.1717	0.2891	37.95
		DA-CLIP	18.53	0.5320	0.5335	0.1916	0.3476	33.87
		InstructIR	17.09	0.5135	0.5582	0.1732	0.2537	33.69
		AutoDIR	18.61	0.5443	0.5019	0.2045	0.2939	37.86
		AgenticIR	18.82	0.5474	0.4493	0.2698	0.3948	48.68
		MAIR	19.42	0.5544	0.4142	0.2798	0.4239	**51.36**
		EvoIR-Agent-I	**21.52**	**0.6354**	**0.4108**	**0.2954**	**0.4448**	**51.36**
	Setting II	4KAgent	19.77	0.5629	0.4271	0.3545	0.5233	55.56
		TIR-Agent	19.53	0.5643	**0.4120**	**0.3739**	**0.5495**	**56.93**
		EvoIR-Agent-II	**22.12**	**0.6588**	0.4528	0.3321	0.4977	55.21

After partitioning P_{new}, we further optimize and iterate on the existing P_{old} through a iteration process between a soft updates to keep up with C_s driven by an agent and a hard constraint to keep up with C_r by Spearmanρ [51]:

$$P_{\text{new}}^{t+1} \leftarrow \text{Iter}\big(P_{\text{new}}^{t}, P_{\text{old}}^{t}; \text{Agent(func)}, \rho\big) \quad \rho(\text{rank}_i, \text{rank}_j) = 1 - \frac{6\sum_{i=1}^{n}\Delta_i^2}{n(n^2-1)}, \tag{13}$$

where *func* denotes the operation functions on P for agent, which includes the following meta operation: add, replace, update and delete. Through negotiation, the iteration process reaches a consensus on appending $\{I_D^{(i)}\}_{i=1}^{m}$ and rectifying the $text$ representation of P.

Following multiple mini-batch learning steps regularized by C_s and C_r, the information within P stabilizes. Consequently, the historically cached ranks associated with the images clustered in the specific P also converge. By leveraging these stable ranks, we derive the final priority function p bound to P, which functions as the priority in fine-grained granularity:

$$p = \text{Stabilize}\left(\text{rank}^{t}\right). \tag{14}$$

Table 2: Quantitative comparison on two real-world settings from the FoundIR benchmark in two *Preference* (Fidelity and Perception). Best, second-best, and third-best results are highlighted as **First**, Second, and Third.

Degrad.	Methods	Fidelity			Perception			Invoc. ↓
		PSNR ↑	SSIM ↑	LPIPS ↓	MANIQA ↑	CLIP-IQA ↑	MUSIQ ↑	
L+N	AgenticIR	11.54	0.5468	0.6285	0.2482	0.3165	40.63	**2.50**
	4KAgent	16.77	0.6410	0.5799	0.2537	0.3052	**44.88**	15.91
	EvoIR-Agent	**17.81**	**0.7093**	**0.5380**	**0.2677**	**0.3506**	42.71	4.73
B+J	AgenticIR	22.66	**0.7113**	0.2115	0.2452	**0.2703**	49.48	3.68
	4KAgent	22.03	0.6959	0.2070	**0.2527**	0.2702	**51.53**	5.04
	EvoIR-Agent	**22.77**	0.7070	**0.1976**	0.2489	0.2633	50.65	**2.02**

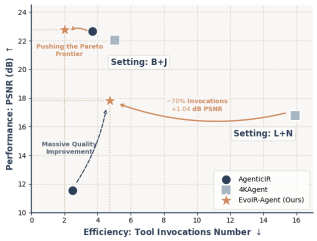

Figure 4: Performance vs. Efficiency trade-off visualization.

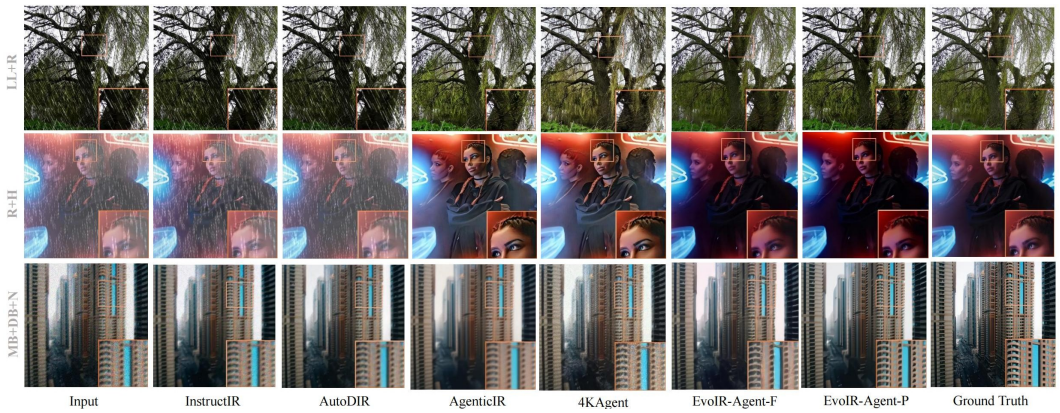

Figure 5: Visual comparison examples on MiO100 dataset. **EvoIR-Agent-F** denoted the fidelity *Preference* requirement, while **EvoIR-Agent-P** denoted the perception *Preference* requirement.

4 Experiments

4.1 Experimental Setup

Test Datasets and Tool Settings. To verify the applicability of **EvoIR-Agent** across different datasets, a comprehensive testing process is conducted using both synthetic and real-world datasets. In the case of the synthesized datasets, the approach delineated in [16] is employed, which contains 1,440 low-quality images that have undergone processing via 16 combinations of two or three types of degradations applied to images from MiO100 [29]. In the case of the real-world dataset, FoundIR [52] is employed for the purpose of testing in two distinct degradation scenarios: low light with noise and blur with JPEG. Each scenario includes 50 real-world image pairs of low-quality inputs and ground-truth targets. The detailed list of settings can be found in Appendix C.

Compared Methods. We compare our method with six AiOIR models: AirNet [7], PromptIR [30], MiOIR [29], DA-CLIP [31], InstructIR [9], and AutoDIR [10]. Furthermore, we compare with four agent-based IR methods: AgenticIR [16], MAIR [19], 4KAgent [20], and TIR-Agent [18]. All the methods above are without a re-training process.

Evaluation Metrics. We evaluate the quality using both full-reference (FR) and no-reference (NR) image quality assessment (IQA) metrics. The FR metrics include PSNR, SSIM [53], and LPIPS [54], while the NR metrics include MANIQA [55], CLIP-IQA [56], and MUSIQ [57].

4.2 Performance Comparison with Other Methods

Comparison with Other Methods. As shown in Table 1, EvoIR-Agent significantly outperforms state-of-the-art methods in Setting I, leading the baselines by an average of 2.35 dB in PSNR and 0.065 in SSIM. In Setting II, while EvoIR-Agent remains highly competitive in FR metrics, some NR metrics are slightly lower than specific baselines. We attribute this to the resource-intensive strategies employed by these baselines: 4KAgent [20] relies on exhaustive tool selection during inference, while TIR-Agent [18] requires training on massive datasets. In contrast, EvoIR-Agent achieves comparable performance with small data samples and remains compatible with tools and degradation. Qualitative

Degrad.	Methods	Invoc. ↓
GroupA	w/o experience	6.38
	w/ coarse	4.67
	w/ fine	**3.45**
GroupC	w/o experience	6.69
	w/ insight	6.37
	w/ coarse	5.04
	w/ fine	**4.32**

(a) Ablation study on experience granularity with different groups.

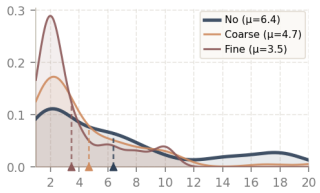

(b) Distribution of tool invocation number on GroupA.

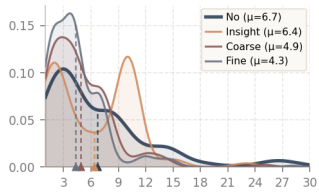

(c) Distribution of tool invocation number on GroupC.

Figure 6: (a) Ablation study on experience granularity with three levels; (b) and (c) visualize the probabilistic density function of the tool invocations frequency distribution on different granularities.

Times	UQI ↑	Total Rb ↓
0	0.0761	2.50
1	0.5830	1.67
2	**0.9824**	**1.29**
3	0.8867	1.51
4	0.9238	1.47

(a) Ablation on evolving times on GroupB of the MiO100 dataset with batch size $B = 25$.

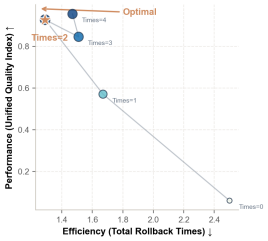

(b) Cost-Quality Trade-off.

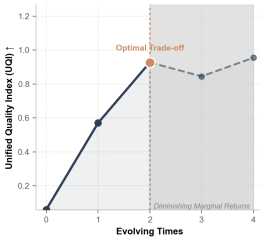

(c) Quality Progression.

Figure 7: Performance-Efficiency analysis of the self-evolving process. (a) Quantitative ablation on evolution times for performance (Unified Quality Index, which averaged across six IQA metrics for better evaluation) and efficiency (Total Rollback Times). (b) Cost-quality Pareto front between performance and efficiency. (b) Quality progression over evolution times.

results in Figure 5 further confirm that our method effectively mitigates under degradation coupling scenarios while maintaining the *Preference* (Fidelity and Perception) as an experience component.

Generalization to Real-World Scenarios. Table 2 evaluates the zero-shot generalization of EvoIR-Agent on the real-world FoundIR dataset [52]. Our method consistently surpasses existing open-source IRA approaches in restoration quality. As shown in Figure 4, when considering the tool invocation numbers, EvoIR-Agent establishes a Pareto-optimal trade-off between restoration performance and inference efficiency. Specifically, it outperforms the strongest baselines by up to +1.04 dB in PSNR while simultaneously slashing tool invocation number by 70%.

4.3 Ablation Study

Evaluation on the hierarchical experience pool. As shown in Figure 6, when the granularity transitions from insight to fine, the tool invocation numbers decrease substantially. Crucially, the probability density distribution of tool invocation numbers shifts markedly toward the lower-invocation regime, indicating that finer experience enables more precise guidance. A comprehensive examination of the hierarchy experience trade-off is provided in Appendix B.3.

Evaluation on the evolution times. As shown in Figure 7, Times $= 2$ emerges as the optimal sweet spot between performance (represented by Unified Quality Index) and efficiency (represented by Total Rollback Times). The self-evolving experience mechanism not only enhances the performance but also drastically reduces inference latency during substantial learning on the data source. A comprehensive examination of these factors is provided in Appendix B.5.

5 Conclusion

In this paper, we address a critical dilemma in Image Restoration Agent (IRA) for the experience design: the limited compatibility of training-based methods versus the inference inefficiency of training-free paradigms. To resolve this, we propose **EvoIR-Agent**, which employs a hierarchical experience pool to provide coarse-to-fine guidance for three experience components. Furthermore, we introduce a self-evolving mechanism that iteratively refines this experience pool using accumulated records. This continuous evolution enables the achievement of a balance between restoration quality and efficiency. Extensive experiments demonstrate that we successfully bridge the gap between existing paradigms by its self-evolving experience-driven learning capacity.

Acknowledgments

This work was supported by the National Natural Science Foundation of China under Grant U24A20251, 62071500, Shenzhen Science and Technology Program under Grant.

References

[1] Kai Zhang, Wangmeng Zuo, Yunjin Chen, Deyu Meng, and Lei Zhang. Beyond a gaussian denoiser: Residual learning of deep cnn for image denoising. *IEEE transactions on image processing*, 26(7): 3142–3155, 2017.

[2] Xintao Wang, Ke Yu, Shixiang Wu, Jinjin Gu, Yihao Liu, Chao Dong, Yu Qiao, and Chen Change Loy. Esrgan: Enhanced super-resolution generative adversarial networks. In *Proceedings of the European conference on computer vision (ECCV) workshops*, pages 0–0, 2018.

[3] Xin Tao, Hongyun Gao, Xiaoyong Shen, Jue Wang, and Jiaya Jia. Scale-recurrent network for deep image deblurring. In *Proceedings of the IEEE conference on computer vision and pattern recognition*, pages 8174–8182, 2018.

[4] Zhi Jin, Yuwei Qiu, Kaihao Zhang, Hongdong Li, and Wenhan Luo. Mb-taylorformer v2: Improved multi-branch linear transformer expanded by taylor formula for image restoration. *IEEE Transactions on Pattern Analysis and Machine Intelligence*, 2025.

[5] Chenxi Wang, Hongjun Wu, and Zhi Jin. Fourllie: Boosting low-light image enhancement by fourier frequency information. In *Proceedings of the 31st ACM international conference on multimedia*, pages 7459–7469, 2023.

[6] Junjun Jiang, Zengyuan Zuo, Gang Wu, Kui Jiang, and Xianming Liu. A survey on all-in-one image restoration: Taxonomy, evaluation and future trends. *IEEE Transactions on Pattern Analysis and Machine Intelligence*, 2025.

[7] Ruoteng Li, Robby T Tan, and Loong-Fah Cheong. All in one bad weather removal using architectural search. In *Proceedings of the IEEE/CVF conference on computer vision and pattern recognition*, pages 3175–3185, 2020.

[8] Jeya Maria Jose Valanarasu, Rajeev Yasarla, and Vishal M Patel. Transweather: Transformer-based restoration of images degraded by adverse weather conditions. In *Proceedings of the IEEE/CVF conference on computer vision and pattern recognition*, pages 2353–2363, 2022.

[9] Marcos V Conde, Gregor Geigle, and Radu Timofte. Instructir: High-quality image restoration following human instructions. In *European Conference on Computer Vision*, pages 1–21. Springer, 2024.

[10] Yitong Jiang, Zhaoyang Zhang, Tianfan Xue, and Jinwei Gu. Autodir: Automatic all-in-one image restoration with latent diffusion. In *European Conference on Computer Vision*, pages 340–359. Springer, 2024.

[11] Yunlong Lin, Zixu Lin, Haoyu Chen, Panwang Pan, Chenxin Li, Sixiang Chen, Kairun Wen, Yeying Jin, Wenbo Li, and Xinghao Ding. Jarvisir: Elevating autonomous driving perception with intelligent image restoration. In *Proceedings of the IEEE/CVF Conference on Computer Vision and Pattern Recognition*, pages 22369–22380, 2025.

[12] Jiawei Wu, Zhifei Yang, Zhe Wang, and Zhi Jin. Gradient as conditions: Rethinking hog for all-in-one image restoration. In *Proceedings of the AAAI Conference on Artificial Intelligence*, volume 40, pages 10682–10690, 2026.

[13] Peng Wang, Shuai Bai, Sinan Tan, Shijie Wang, Zhihao Fan, Jinze Bai, Keqin Chen, Xuejing Liu, Jialin Wang, Wenbin Ge, et al. Qwen2-vl: Enhancing vision-language model's perception of the world at any resolution. *arXiv preprint arXiv:2409.12191*, 2024.

[14] Jingyi Zhang, Jiaxing Huang, Sheng Jin, and Shijian Lu. Vision-language models for vision tasks: A survey. *IEEE transactions on pattern analysis and machine intelligence*, 46(8):5625–5644, 2024.

[15] Haoyu Chen, Wenbo Li, Jinjin Gu, Jingjing Ren, Sixiang Chen, Tian Ye, Renjing Pei, Kaiwen Zhou, Fenglong Song, and Lei Zhu. Restoreagent: Autonomous image restoration agent via multimodal large language models. *Advances in Neural Information Processing Systems*, 37:110643–110666, 2024.

[16] Kaiwen Zhu, Jinjin Gu, Zhiyuan You, Yu Qiao, and Chao Dong. An intelligent agentic system for complex image restoration problems. In *The Thirteenth International Conference on Learning Representations*.

[17] Jianglin Lu, Yuanwei Wu, Ziyi Zhao, Hongcheng Wang, Felix Jimenez, Abrar Majeedi, and Yun Fu. Simplecall: A lightweight image restoration agent in label-free environments with mllm perceptual feedback. *arXiv preprint arXiv:2512.18599*, 2025.

[18] Yisheng Zhang, Guoli Jia, Haote Hu, Shanxu Zhao, Kaikai Zhao, Long Sun, Xinwei Long, Kai Tian, Che Jiang, Zhaoxiang Liu, et al. Tir-agent: Training an explorative and efficient agent for image restoration. *arXiv preprint arXiv:2603.27742*, 2026.

[19] Xu Jiang, Gehui Li, Bin Chen, and Jian Zhang. Multi-agent image restoration. *arXiv preprint arXiv:2503.09403*, 2025.

[20] Yushen Zuo, Qi Zheng, Mingyang Wu, Xinrui Jiang, Renjie Li, Jian Wang, Yide Zhang, Gengchen Mai, Lihong Wang, James Zou, et al. 4kagent: Agentic any image to 4k super-resolution. In *The Thirty-ninth Annual Conference on Neural Information Processing Systems*.

[21] Andrew Zhao, Daniel Huang, Quentin Xu, Matthieu Lin, Yong-Jin Liu, and Gao Huang. Expel: Llm agents are experiential learners. In *Proceedings of the AAAI Conference on Artificial Intelligence*, volume 38, pages 19632–19642, 2024.

[22] Qizheng Zhang, Changran Hu, Shubhangi Upasani, Boyuan Ma, Fenglu Hong, Vamsidhar Kamanuru, Jay Rainton, Chen Wu, Mengmeng Ji, Hanchen Li, et al. Agentic context engineering: Evolving contexts for self-improving language models. *arXiv preprint arXiv:2510.04618*, 2025.

[23] Wujiang Xu, Zujie Liang, Kai Mei, Hang Gao, Juntao Tan, and Yongfeng Zhang. A-mem: Agentic memory for llm agents. *arXiv preprint arXiv:2502.12110*, 2025.

[24] Jizhan Fang, Xinle Deng, Haoming Xu, Ziyan Jiang, Yuqi Tang, Ziwen Xu, Shumin Deng, Yunzhi Yao, Mengru Wang, Shuofei Qiao, et al. Lightmem: Lightweight and efficient memory-augmented generation. *arXiv preprint arXiv:2510.18866*, 2025.

[25] Weiquan Huang, Aoqi Wu, Yifan Yang, Xufang Luo, Yuqing Yang, Usman Naseem, Chunyu Wang, Qi Dai, Xiyang Dai, Dongdong Chen, et al. Llm2clip: Powerful language model unlocks richer cross-modality representation. In *Proceedings of the AAAI Conference on Artificial Intelligence*, volume 40, pages 5131–5139, 2026.

[26] Guibin Zhang, Muxin Fu, Kun Wang, Guancheng Wan, Miao Yu, and Shuicheng YAN. G-memory: Tracing hierarchical memory for multi-agent systems. In *The Thirty-ninth Annual Conference on Neural Information Processing Systems*.

[27] Shuo Yu, Mingyue Cheng, Daoyu Wang, Qi Liu, Zirui Liu, Ze Guo, and Xiaoyu Tao. Memweaver: A hierarchical memory from textual interactive behaviors for personalized generation. *arXiv preprint arXiv:2510.07713*, 2025.

[28] Hadi Pouransari, David Grangier, C Thomas, Michael Kirchhof, and Oncel Tuzel. Pretraining with hierarchical memories: separating long-tail and common knowledge. *arXiv preprint arXiv:2510.02375*, 2025.

[29] Xiangtao Kong, Chao Dong, and Lei Zhang. Towards effective multiple-in-one image restoration: A sequential and prompt learning strategy. *arXiv preprint arXiv:2401.03379*, 2024.

[30] Vaishnav Potlapalli, Syed Waqas Zamir, Salman H Khan, and Fahad Shahbaz Khan. Promptir: Prompting for all-in-one image restoration. *Advances in neural information processing systems*, 36:71275–71293, 2023.

[31] Ziwei Luo, Fredrik K Gustafsson, Zheng Zhao, Jens Sjölund, and Thomas B Schön. Controlling vision-language models for universal image restoration. *arXiv preprint arXiv:2310.01018*, 3(8), 2023.

[32] I Chen, Wei-Ting Chen, Yu-Wei Liu, Yuan-Chun Chiang, Sy-Yen Kuo, Ming-Hsuan Yang, et al. Unirestore: Unified perceptual and task-oriented image restoration model using diffusion prior. In *Proceedings of the Computer Vision and Pattern Recognition Conference*, pages 17969–17979, 2025.

[33] Wenyang Luo, Haina Qin, Zewen Chen, Libin Wang, Dandan Zheng, Yuming Li, Yufan Liu, Bing Li, and Weiming Hu. Visual-instructed degradation diffusion for all-in-one image restoration. In *Proceedings of the Computer Vision and Pattern Recognition Conference*, pages 12764–12777, 2025.

[34] Xiaole Tang, Xiaoyi He, Jiayi Xu, Xiang Gu, and Jian Sun. Learning continuous wasserstein barycenter space for generalized all-in-one image restoration. *IEEE Transactions on Pattern Analysis and Machine Intelligence*, 2026.

[35] Yingjie Zhou, Jiezhang Cao, Zicheng Zhang, Farong Wen, Yanwei Jiang, Jun Jia, Xiaohong Liu, Xiongkuo Min, and Guangtao Zhai. Q-agent: quality-driven chain-of-thought image restoration agent through robust multimodal large language model. *arXiv preprint arXiv:2504.07148*, 2025.

[36] Yijian Wang, Qingsen Yan, Jiantao Zhou, Duwei Dai, and Wei Dong. Paagent: Portrait-aware image restoration agent via subjective-objective reinforcement learning. *arXiv preprint arXiv:2603.17055*, 2026.

[37] Bingchen Li, Xin Li, Yiting Lu, and Zhibo Chen. Hybrid agents for image restoration. *arXiv preprint arXiv:2503.10120*, 2025.

[38] Zeyu Zhang, Quanyu Dai, Xiaohe Bo, Chen Ma, Rui Li, Xu Chen, Jieming Zhu, Zhenhua Dong, and Ji-Rong Wen. A survey on the memory mechanism of large language model-based agents. *ACM Transactions on Information Systems*, 43(6):1–47, 2025.

[39] Wei-Chieh Huang, Weizhi Zhang, Yueqing Liang, Yuanchen Bei, Yankai Chen, Tao Feng, Xinyu Pan, Zhen Tan, Yu Wang, Tianxin Wei, et al. Rethinking memory mechanisms of foundation agents in the second half. *arXiv preprint arXiv:2602.06052*, 2026.

[40] Zidi Xiong, Yuping Lin, Wenya Xie, Pengfei He, Zirui Liu, Jiliang Tang, Himabindu Lakkaraju, and Zhen Xiang. How memory management impacts llm agents: An empirical study of experience-following behavior. *arXiv preprint arXiv:2505.16067*, 2025.

[41] Siyu Xia, Zekun Xu, Jiajun Chai, Wentian Fan, Yan Song, Xiaohan Wang, Guojun Yin, Wei Lin, Haifeng Zhang, and Jun Wang. From experience to strategy: Empowering llm agents with trainable graph memory. *arXiv preprint arXiv:2511.07800*, 2025.

[42] Qirui Mi, Zhijian Ma, Mengyue Yang, Haoxuan Li, Yisen Wang, Haifeng Zhang, and Jun Wang. Procmem: Learning reusable procedural memory from experience via non-parametric ppo for llm agents. *arXiv preprint arXiv:2602.01869*, 2026.

[43] Zouying Cao, Jiaji Deng, Li Yu, Weikang Zhou, Zhaoyang Liu, Bolin Ding, and Hai Zhao. Remember me, refine me: A dynamic procedural memory framework for experience-driven agent evolution. *arXiv preprint arXiv:2512.10696*, 2025.

[44] Zhicheng Cai, Xinyuan Guo, Yu Pei, Jiangtao Feng, Jinsong Su, Jiangjie Chen, Ya-Qin Zhang, Wei-Ying Ma, Mingxuan Wang, and Hao Zhou. Flex: Continuous agent evolution via forward learning from experience. *arXiv preprint arXiv:2511.06449*, 2025.

[45] Jiaqi Liu, Yaofeng Su, Peng Xia, Siwei Han, Zeyu Zheng, Cihang Xie, Mingyu Ding, and Huaxiu Yao. Simplemem: Efficient lifelong memory for llm agents. *arXiv preprint arXiv:2601.02553*, 2026.

[46] Roger R Davidson. On extending the bradley-terry model to accommodate ties in paired comparison experiments. *Journal of the American Statistical Association*, 65(329):317–328, 1970.

[47] Abraham Wald. Tests of statistical hypotheses concerning several parameters when the number of observations is large. *Transactions of the American Mathematical society*, 54(3):426–482, 1943.

[48] Chi-Min Chan, Weize Chen, Yusheng Su, Jianxuan Yu, Wei Xue, Shanghang Zhang, Jie Fu, and Zhiyuan Liu. Chateval: Towards better llm-based evaluators through multi-agent debate. In *The Twelfth International Conference on Learning Representations*.

[49] Andries Petrus Smit, Nathan Grinsztajn, Paul Duckworth, Thomas D Barrett, and Arnu Pretorius. Should we be going mad? a look at multi-agent debate strategies for llms. In *International Conference on Machine Learning*, pages 45883–45905. PMLR, 2024.

[50] Anand S Rao, Michael P Georgeff, et al. Bdi agents: from theory to practice. In *Icmas*, volume 95, pages 312–319, 1995.

[51] The proof and measurement of association between two things. 1961.

[52] Hao Li, Xiang Chen, Jiangxin Dong, Jinhui Tang, and Jinshan Pan. Foundir: Unleashing million-scale training data to advance foundation models for image restoration. In *Proceedings of the IEEE/CVF international conference on computer vision*, pages 12626–12636, 2025.

[53] Zhou Wang, Alan C Bovik, Hamid R Sheikh, and Eero P Simoncelli. Image quality assessment: from error visibility to structural similarity. *IEEE transactions on image processing*, 13(4):600–612, 2004.

[54] Richard Zhang, Phillip Isola, Alexei A Efros, Eli Shechtman, and Oliver Wang. The unreasonable effectiveness of deep features as a perceptual metric. In *Proceedings of the IEEE conference on computer vision and pattern recognition*, pages 586–595, 2018.

[55] Sidi Yang, Tianhe Wu, Shuwei Shi, Shanshan Lao, Yuan Gong, Mingdeng Cao, Jiahao Wang, and Yujiu Yang. Maniqa: Multi-dimension attention network for no-reference image quality assessment. In *Proceedings of the IEEE/CVF conference on computer vision and pattern recognition*, pages 1191–1200, 2022.

[56] Jianyi Wang, Kelvin CK Chan, and Chen Change Loy. Exploring clip for assessing the look and feel of images. In *Proceedings of the AAAI conference on artificial intelligence*, volume 37, pages 2555–2563, 2023.

[57] Junjie Ke, Qifei Wang, Yilin Wang, Peyman Milanfar, and Feng Yang. Musiq: Multi-scale image quality transformer. In *Proceedings of the IEEE/CVF international conference on computer vision*, pages 5148–5157, 2021.

[58] Zhiyuan You, Zheyuan Li, Jinjin Gu, Zhenfei Yin, Tianfan Xue, and Chao Dong. Depicting beyond scores: Advancing image quality assessment through multi-modal language models. In *European Conference on Computer Vision*, pages 259–276. Springer, 2024.

[59] Haoning Wu, Zicheng Zhang, Weixia Zhang, Chaofeng Chen, Liang Liao, Chunyi Li, Yixuan Gao, Annan Wang, Erli Zhang, Wenxiu Sun, et al. Q-align: teaching lmms for visual scoring via discrete text-defined levels. In *Proceedings of the 41st International Conference on Machine Learning*, pages 54015–54029, 2024.

[60] Ali M Reza. Realization of the contrast limited adaptive histogram equalization (clahe) for real-time image enhancement. *Journal of VLSI signal processing systems for signal, image and video technology*, 38(1): 35–44, 2004.

[61] Lingyan Ruan, Bin Chen, Jizhou Li, and Miuling Lam. Learning to deblur using light field generated and real defocus images. In *Proceedings of the IEEE/CVF conference on computer vision and pattern recognition*, pages 16304–16313, 2022.

[62] Junyong Lee, Hyeongseok Son, Jaesung Rim, Sunghyun Cho, and Seungyong Lee. Iterative filter adaptive network for single image defocus deblurring. In *Proceedings of the IEEE/CVF conference on computer vision and pattern recognition*, pages 2034–2042, 2021.

[63] Syed Waqas Zamir, Aditya Arora, Salman Khan, Munawar Hayat, Fahad Shahbaz Khan, and Ming-Hsuan Yang. Restormer: Efficient transformer for high-resolution image restoration. In *Proceedings of the IEEE/CVF conference on computer vision and pattern recognition*, pages 5728–5739, 2022.

[64] Jingyun Liang, Jiezhang Cao, Guolei Sun, Kai Zhang, Luc Van Gool, and Radu Timofte. Swinir: Image restoration using swin transformer. In *Proceedings of the IEEE/CVF international conference on computer vision*, pages 1833–1844, 2021.

[65] Jiaxi Jiang, Kai Zhang, and Radu Timofte. Towards flexible blind jpeg artifacts removal. In *Proceedings of the IEEE/CVF International Conference on Computer Vision*, pages 4997–5006, 2021.

[66] Zhengzhong Tu, Hossein Talebi, Han Zhang, Feng Yang, Peyman Milanfar, Alan Bovik, and Yinxiao Li. Maxim: Multi-axis mlp for image processing. In *Proceedings of the IEEE/CVF conference on computer vision and pattern recognition*, pages 5769–5780, 2022.

[67] Syed Waqas Zamir, Aditya Arora, Salman Khan, Munawar Hayat, Fahad Shahbaz Khan, Ming-Hsuan Yang, and Ling Shao. Multi-stage progressive image restoration. In *Proceedings of the IEEE/CVF conference on computer vision and pattern recognition*, pages 14821–14831, 2021.

[68] Xiangyu Chen, Zheyuan Li, Yuandong Pu, Yihao Liu, Jiantao Zhou, Yu Qiao, and Chao Dong. A comparative study of image restoration networks for general backbone network design. In *European Conference on Computer Vision*, pages 74–91. Springer, 2024.

[69] Rui-Qi Wu, Zheng-Peng Duan, Chun-Le Guo, Zhi Chai, and Chongyi Li. Ridcp: Revitalizing real image dehazing via high-quality codebook priors. In *Proceedings of the IEEE/CVF conference on computer vision and pattern recognition*, pages 22282–22291, 2023.

[70] Yuda Song, Zhuqing He, Hui Qian, and Xin Du. Vision transformers for single image dehazing. *IEEE Transactions on Image Processing*, 32:1927–1941, 2023.

[71] Xinqi Lin, Jingwen He, Ziyan Chen, Zhaoyang Lyu, Bo Dai, Fanghua Yu, Yu Qiao, Wanli Ouyang, and Chao Dong. Diffbir: Toward blind image restoration with generative diffusion prior. In *European conference on computer vision*, pages 430–448. Springer, 2024.

[72] Xiangyu Chen, Xintao Wang, Wenlong Zhang, Xiangtao Kong, Yu Qiao, Jiantao Zhou, and Chao Dong. Hat: Hybrid attention transformer for image restoration. *IEEE Transactions on Pattern Analysis and Machine Intelligence*, 2025.

[73] Yuhao Liu, Zhanghan Ke, Fang Liu, Nanxuan Zhao, and Rynson WH Lau. Diff-plugin: Revitalizing details for diffusion-based low-level tasks. In *Proceedings of the IEEE/CVF Conference on Computer Vision and Pattern Recognition*, pages 4197–4208, 2024.

[74] Xiaoqian Lv, Shengping Zhang, Chenyang Wang, Yichen Zheng, Bineng Zhong, Chongyi Li, and Liqiang Nie. Fourier priors-guided diffusion for zero-shot joint low-light enhancement and deblurring. In *Proceedings of the IEEE/CVF conference on computer vision and pattern recognition*, pages 25378–25388, 2024.

[75] Yuning Cui, Wenqi Ren, Xiaochun Cao, and Alois Knoll. Revitalizing convolutional network for image restoration. *IEEE Transactions on Pattern Analysis and Machine Intelligence*, 46(12):9423–9438, 2024.

[76] Yuning Cui, Wenqi Ren, and Alois Knoll. Omni-kernel network for image restoration. In *Proceedings of the AAAI conference on artificial intelligence*, volume 38, pages 1426–1434, 2024.

[77] Liangyu Chen, Xiaojie Chu, Xiangyu Zhang, and Jian Sun. Simple baselines for image restoration. In *European conference on computer vision*, pages 17–33. Springer, 2022.

[78] Lingshun Kong, Jiangxin Dong, Jinhui Tang, Ming-Hsuan Yang, and Jinshan Pan. Efficient visual state space model for image deblurring. In *Proceedings of the computer vision and pattern recognition conference*, pages 12710–12719, 2025.

[79] Chih-Chung Hsu, Chia-Ming Lee, and Yi-Shiuan Chou. Drct: Saving image super-resolution away from information bottleneck. In *Proceedings of the IEEE/CVF conference on computer vision and pattern recognition*, pages 6133–6142, 2024.

[80] Shu-Chuan Chu, Zhi-Chao Dou, Jeng-Shyang Pan, Shaowei Weng, and Junbao Li. Hmanet: Hybrid multi-axis aggregation network for image super-resolution. In *Proceedings of the IEEE/CVF conference on computer vision and pattern recognition*, pages 6257–6266, 2024.

[81] Rongyuan Wu, Lingchen Sun, Zhiyuan Ma, and Lei Zhang. One-step effective diffusion network for real-world image super-resolution. *Advances in Neural Information Processing Systems*, 37:92529–92553, 2024.

[82] Lingchen Sun, Rongyuan Wu, Zhiyuan Ma, Shuaizheng Liu, Qiaosi Yi, and Lei Zhang. Pixel-level and semantic-level adjustable super-resolution: A dual-lora approach. In *Proceedings of the IEEE/CVF Conference on Computer Vision and Pattern Recognition*, pages 2333–2343, 2025.

[83] Dafeng Zhang, Feiyu Huang, Shizhuo Liu, Xiaobing Wang, and Zhezhu Jin. Swinfir: Revisiting the swinir with fast fourier convolution and improved training for image super-resolution. *arXiv preprint arXiv:2208.11247*, 2022.

[84] An Yang, Anfeng Li, Baosong Yang, Beichen Zhang, Binyuan Hui, Bo Zheng, Bowen Yu, Chang Gao, Chengen Huang, Chenxu Lv, et al. Qwen3 technical report. *arXiv preprint arXiv:2505.09388*, 2025.

A Additional Proofs

A.1 Experience Foundation Proving

Findings on 1. By conducting a thorough examination of the restored images on [16, 20], we observe a phenomenon. Since [16, 20] utilizes a heuristic strategy to select a tool for each degradation type, the restoration procedure is terminated once the degradation has been removed. Consequently, multiple iterations of the same process may yield different restored images, and they often exhibit noticeable differences in visual quality, as demonstrated in Figure 8. This phenomenon motivates the introduction of *Preference* as an experience component in the IRA, denoted as Q. This is a configurable feature for human utilization. We instantiate them using two widely adopted criteria in IR from score-based IQA: *Fidelity* and *Perceptual*. More generally, it is believed that language-based IQA [58, 59] would better align with human preferences.

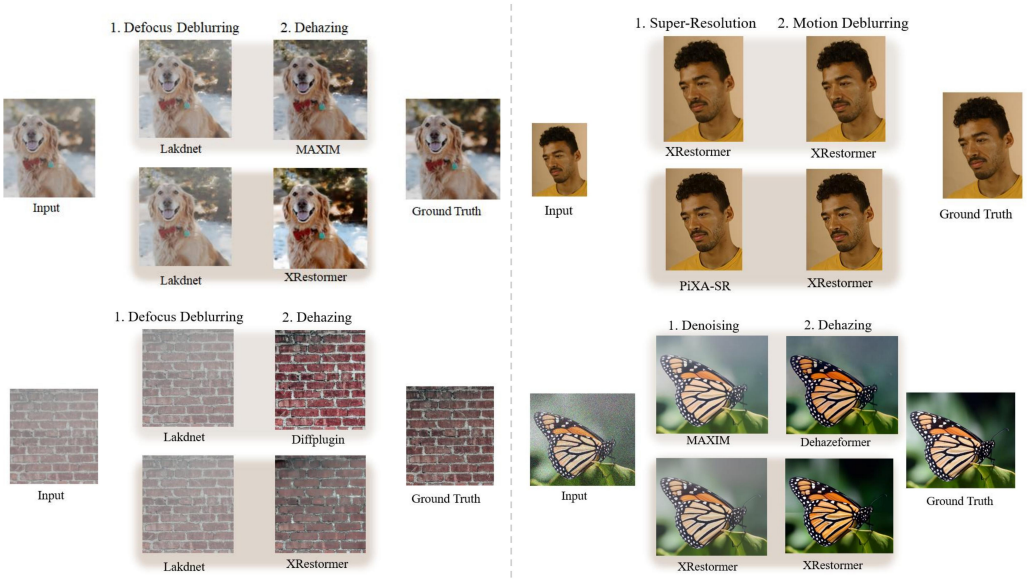

Figure 8: Visualization of *Preference* setting. It has been demonstrated that, in instances where image restoration is achieved, the visual quality of the restored image can vary with different tools.

Findings on 2. Under degradation coupling setting, jointly exploring the tool T choices and degradation removal order O typically leads to a computationally prohibitive permutational space for experience modeling. We conduct a series of experiments to seek insight. To evaluate the impact of degradation removal order under degradation coupling setting, we comprehensively assess performance across 10 distinct IQA metrics within the MiO100 [29] dataset. As illustrated in Figure 9, the correct removal order (represented by dashed lines) establishes a Pareto-optimal front across the diverse IQA landscape. However, an improper removal order (represented by solid lines) invariably bottlenecks the performance, which cannot be salvaged even by employing the optimal tool. Conversely, pairing sub-optimal tools with an incorrect order only further drops in metrics.

Consequently, we propose a simplified, decoupled construction paradigm. By persistently anchoring our choice to the optimal tool τ^* in preference Q, we reduce the intractable joint optimization from a vast $\prod_{d_i \in D} \mathcal{T}(d_i)$ search space down to a purely D-centric permutation problem, which depends solely on the degradation types D in preference Q under degradation coupling setting. Subsequently, the experience modeling process will be concise and straightforward. This also inspires us to establish the rollback process being executed in O before T to keep the integrity of experience guidance.

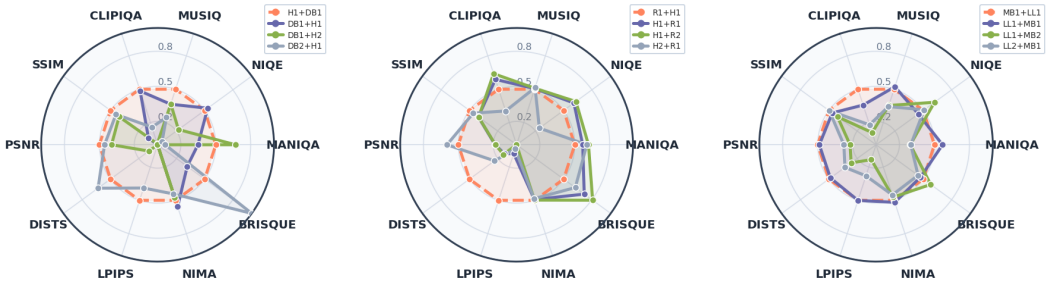

(a) Defocus Blur + Haze (b) Rain + Haze (c) Low light + Motion Blur

Figure 9: Experiments conducted on the MiO100 dataset and the resulting radar chart. It demonstrates that in the degradation coupling setting, the degradation removal order O yields greater benefits than the tool T selection. All metrics are normalized and maximized based on the optimal degradation removal order (dashed line).

B Additional Experiments

B.1 Ablation Studies on Rollback Mechanism and Preference Setting

Evaluation on rollback mechanism. The left of Table 3 illustrates that, in nearly all instances, the metrics with the rollback process are superior. Notably, the rollback process differs from [16, 20], as our method is structured around the experience pool. Consequently, we initiate the rollback process on O and subsequently on T to maintain the integrity of the experience guidance.

Evaluation on preference setting. The right of Table 3 clearly demonstrates that fidelity consistently achieves superior FR metrics except LPIPS, which may focus more on the emphasis on perception quality, while *Perception* dominates in NR metrics across three groups in the MiO100 dataset. It is noteworthy that even when prioritizing perception preference, its FR metrics demonstrate superiority over those of existing state-of-the-art methods.

Table 3: Ablation study on rollback mechanism and preference design with **EvoIR-Agent**.

Degrad.	Rollback Mechanism							Preference Setting						
	Method	PSNR ↑	SSIM ↑	LPIPS ↓	MANIQA ↑	CLIP-IQA ↑	MUSIQ ↑	Dim	PSNR ↑	SSIM ↑	LPIPS ↓	MANIQA ↑	CLIP-IQA ↑	MUSIQ ↑
Group A	w/o Rb.	23.38	0.7410	0.3177	**0.3660**	**0.5214**	61.59	F	**23.86**	**0.7488**	0.3085	0.2833	0.4190	54.37
	w Rb.	**23.86**	**0.7488**	**0.3085**	0.3623	0.5204	**61.82**	P	22.31	0.7103	**0.2831**	**0.3623**	**0.5204**	**61.82**
Group B	w/o Rb.	22.93	0.7582	0.3162	**0.3814**	**0.5436**	61.62	F	**23.38**	**0.7643**	0.3117	0.2727	0.4247	53.28
	w Rb.	**23.38**	**0.7643**	**0.3117**	0.3735	0.5296	**61.96**	P	22.52	0.7392	**0.2694**	**0.3735**	**0.5296**	**61.96**
Group C	w/o Rb.	21.98	0.6576	0.4682	0.3278	0.4930	52.96	F	**22.12**	**0.6588**	0.4528	0.2032	0.3201	41.36
	w Rb.	**22.12**	**0.6588**	**0.4528**	**0.3321**	**0.4977**	**55.21**	P	20.69	0.6004	**0.4072**	**0.3321**	**0.4977**	**55.21**

B.2 Ablating Study for Out-of-Distribution Dataset Adaptability

Table 4 and Figure 10 demonstrate the adaptability of the self-evolving experience mechanism in EvoIR-Agent when confronted with entirely different data domains. The evaluation is conducted on the FoundIR [52] dataset, comprising a total of 50 images in each degradation coupling scenario. We partition the dataset into 20 images allocated for the self-evolution process and the remaining 30 images reserved for testing. To systematically analyze this adaptability, we design three variants:

(1) **EvoIR-Agent-Z:** directly applies the experience gathered from the MiO100 dataset to the OOD scenario for zero-shot testing.

(2) **EvoIR-Agent-T:** leverages the prior experience and continues to finish self-evolving using the 20 images from the OOD dataset for transfer learning.

(3) **EvoIR-Agent-S:** initializes the self-evolving process entirely from scratch using 20 OOD images, devoid of any prior experience.

To comprehensively reflect the performance, we derive a *Unified Quality Index (UQI)* by maximizing, min-max normalizing, and averaging across six IQA metrics (PSNR, SSIM, LPIPS, MANIQA, CLIP-IQA, and MUSIQ). Meanwhile, efficiency is evaluated using the *Total Rollback Times*.

Performance adaptability: As illustrated in (a), EvoIR-Agent-S consistently achieves the highest UQI across both OOD scenarios. Conversely, EvoIR-Agent-Z suffers a significant performance drop in the L+N scenario (UQI: 0.10), indicating that zero-shot application of prior experience results in suboptimal guidance when confronting significantly out-of-distribution data domain. While EvoIR-Agent-T improves upon the zero-shot baseline, it remains inferior to EvoIR-Agent-S. **Efficiency adaptability:** (b) reveals a similar phenomenon. Both suggest adaptability in the performance and efficiency of our self-evolving experience mechanism. **Adaptation trajectory:** (c) clearly maps the holistic trade-off between performance (↑) and efficiency (↓) during the adaptation process. For both degradation scenarios, the evolving trajectory consistently pushes towards this Pareto-optimal region as we transition from EvoIR-Agent-Z to EvoIR-Agent-S.

Table 4: Ablation study on OOD dataset adaptability with **EvoIR-Agent**. The best results are highlighted in **bold**. The derived metrics are highlighted with a shaded background.

Degrad.	Methods	Quality Metrics						Summary	Efficiency Metrics			Summary
		PSNR ↑	SSIM ↑	LPIPS ↓	MANIQA ↑	CLIP-IQA ↑	MUSIQ ↑	UQI ↑	Invoc. ↓	$\mathcal{O}$-Rb ↓	$\mathcal{T}$-Rb ↓	Total Rb ↓
L+N	EvoIR-Agent-G	17.93	0.7064	0.5428	0.1926	0.2212	38.41	0.10	4.30	1.30	0.74	2.04
	EvoIR-Agent-T	16.78	0.6575	0.5841	0.2842	**0.2962**	43.53	0.30	3.55	0.90	0.83	1.73
	EvoIR-Agent-S	**24.50**	**0.8272**	**0.3332**	**0.2851**	0.2733	**44.65**	**0.67**	**2.53**	**0.42**	**0.25**	**0.67**
B+J	EvoIR-Agent-G	23.15	0.6757	0.2063	0.2599	0.2991	51.15	0.73	2.60	0.80	1.60	2.40
	EvoIR-Agent-T	**23.17**	0.6765	0.2090	0.2681	**0.3145**	51.16	0.77	2.43	0.70	1.36	2.07
	EvoIR-Agent-S	23.14	**0.6769**	**0.2055**	**0.2807**	0.2954	52.80	**0.78**	**2.33**	0.67	**1.33**	**2.00**

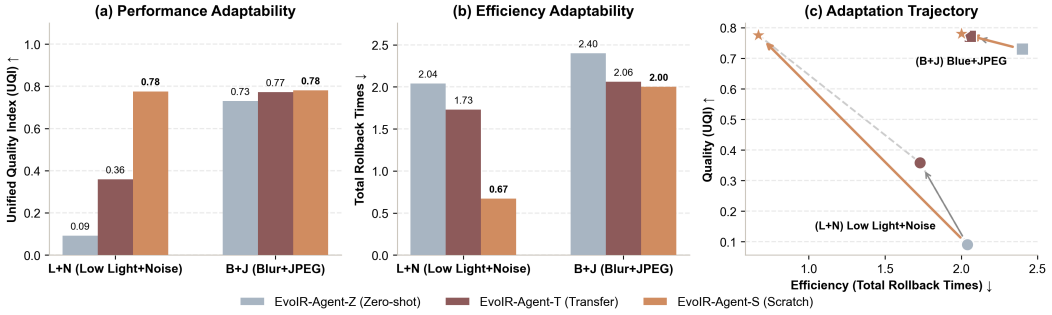

Figure 10: Adaptability analysis of EvoIR-Agent variants across out-of-domain (OOD) dataset. The figure illustrates the (a) performance adaptability measured by the *Unified Quality Index (UQI)*, (b) efficiency adaptability evaluated by the *Total Rollback Times*, and (c) overall adaptation trajectories of the Zero-shot, Transfer, and Scratch variants.

B.3 Detail Ablation Study on Hierarchical Experience Pool

Table 5 and Figure 11 clearly illustrate the impact of experience guidance at different granularities (Times $= 2$). To ensure a fair comparison with consistently processed images, this experiment is conducted on degradation types D, which inherently necessitates fine-grained experience.

As demonstrated, the absence of prior experience forces the system into blind exploration, leading to frequent rollbacks. The introduction of *Insight* experience provides a global fallback mechanism, substantially reducing computational overhead. Efficiency is further enhanced as the granularity refines to *Coarse* and *Fine* levels, while the quality scores remain comparable.

While *Fine-grained* experience offers the highest theoretical efficiency, relying on it may introduce three risks: (i) **Semantic Dependency:** Fine-grained experience relies heavily on the visual perception capability of MLLMs. If the comprehension of MLLM is limited, the *Pattern Profile Learning System* (Sec. 3.4) may fail to generate accurate profiles, leading to planning instability. (ii) **Visual Ambiguity:** For degradations lacking salient visual features, the image encoder [25] struggles to extract discriminative representations. This results in erroneous experience retrieval, where the agent reuses experience from mismatched degradation patterns. (iii) **API Overhead:** Relying on fine-grained experience will incur an API cost, as shown in Table 10.

Conversely, *Coarse-grained* experience circumvents these issues by providing a broader, more robust mapping that is less sensitive to encoder noise, MLLM perceptual errors, or API cost. Therefore, our

hierarchical design achieves an optimal equilibrium: coarse-grained experience ensures generalizable stability, while fine-grained experience drives peak inference efficiency.

Table 5: Detailed ablation study on experience granularity on MiO100 dataset with **EvoIR-Agent**.

Degrad.	Methods	Quality Metrics						Efficiency Metrics			
		PSNR ↑	SSIM ↑	LPIPS ↓	MANIQA ↑	CLIP-IQA ↑	MUSIQ ↑	Invoc. ↓	$\mathcal{O}$-Rb ↓	$\mathcal{T}$-Rb ↓	Total Rb ↓
GroupA	w/o experience	22.12	0.7451	0.2622	0.3438	0.5035	61.63	6.38	1.07	2.20	3.27
	w/ coarse	22.41	**0.7476**	**0.2474**	0.3503	0.5054	**62.86**	4.67	0.79	1.10	1.89
	w/ fine	**22.42**	0.7464	0.2495	**0.3508**	**0.5080**	62.73	**3.45**	**0.59**	**0.81**	**1.40**
GroupB	w/o experience	21.02	0.7923	0.2733	**0.4081**	**0.5858**	63.21	7.13	0.86	2.88	3.74
	w/ insight	21.56	0.8103	0.2604	0.3933	0.5408	64.58	5.00	1.00	1.61	2.61
	w/ coarse	22.20	0.8134	0.2620	0.3913	0.5317	64.55	4.08	0.78	0.68	1.46
	w/ fine	**22.44**	**0.8165**	**0.2576**	0.3941	0.5256	**64.73**	**3.72**	**0.67**	**0.66**	**1.33**
GroupC	w/o experience	21.20	0.5745	0.5364	0.1833	0.2399	35.98	6.69	1.04	1.94	2.98
	w/ insight	21.96	0.5801	0.5770	0.1968	0.2811	37.48	6.37	**0.62**	2.35	2.97
	w/ coarse	**22.15**	**0.5943**	0.5130	**0.2037**	**0.2865**	40.57	5.04	1.01	1.11	2.12
	w/ fine	**22.15**	0.5942	**0.5123**	0.2031	0.2850	**41.09**	**4.32**	0.85	**0.89**	**1.74**

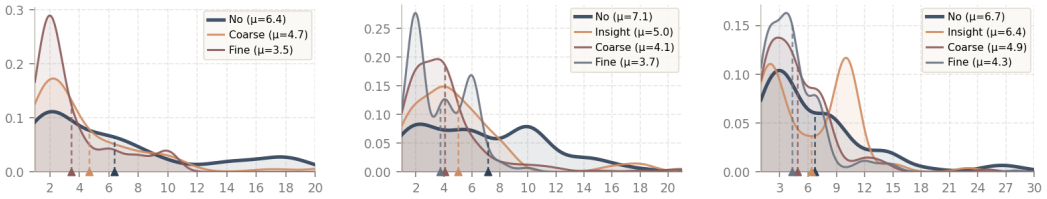

(a) Visualization of invocation number distribution on GroupA.

(b) Visualization of invocation number distribution on GroupB.

(c) Visualization of invocation number distribution on GroupC.

Figure 11: A visualization of the frequency distribution of tool invocation numbers on different experience granularity among GroupA-C

B.4 Visualization on Hierarchical Experience

In this section, we will present several sample sections (insight: Table 6; coarse-grained: Table 7; fine-grained: Table 8) of the hierarchical experience pool to facilitate comprehension. Furthermore, a graph will be constructed to visualize the BTD statistical model underlying the findings, as shown in Figure 12 and Figure 13. It has been demonstrated that by employing a comprehensive approach to acquire the atomic experience component, in conjunction with the statistical properties of the BTD model, a complete graph can be constructed to serve as the core for coarse-grained experience. As illustrated, the size of the nodes corresponds to the ability parameter as estimated by the BTD model. In instances where the coarse-grained experience is uncertain (represented by a dashed line), thereby signifying that fine-grained experience must be utilized as a substitute.

Table 6: Experience sample of **Insight**

Preference	Experience
Fidelity	Here is the reference information from past trials: A reasonable overall elimination order that respects all strong constraints and most weaker ones is: JPEG artifacts → Defocus blur → Haze → Rain → Motion blur → Brightening → Denoising → Super-resolution.
Perception	Here is the reference information from past trials: Recommended "default" sequence, JPEG compression artifacts removal -> Defocus deblurring -> Dehazing -> Deraining -> Super-resolution -> Motion deblurring -> Denoising (only confidently "after JPEG" and "before brightening"

Table 7: Experience sample of **Coarse-grained Experience**

Degradation	Preference	Experience

Motion Blur	Fidelity	`"degradation_type": "motion blur",`
		`"preference": "fidelity",`
		`"ranking": {`
		`"mprnet": 1,`
		`"restormer": 2,`
		`"xrestormer": 3,`
		`"nafnet": 4,`
		`"EVSSM": 5,`
		`"maxim": 6}`

	Perception	`"degradation_type": "motion blur",`
		`"preference": "perception",`
		`"ranking": {`
		`"xrestormer": 1,`
		`"restormer": 2,`
		`"EVSSM": 3,`
		`"mprnet": 4,`
		`"maxim": 5,`
		`"nafnet": 6}`

D+M	Fidelity	`"degradation_type": "dark+motion blur",`
		`"preference": "fidelity",`
		`"ranking": {`
		`"motion blur -> dark": 1,`
		`"dark -> motion blur": 2}`

	Perception	`"degradation_type": "dark+motion blur",`
		`"preference": "perception",`
		`"ranking": {`
		`"dark -> motion blur": 1,`
		`"motion blur -> dark": 2}`

Table 8: Experience sample of **Fine-grained Experience**

Degradation	Preference	Experience
Motion Blur	Fidelity	{ "exp_id": 0, "degradation_type": "motion blur", "preference": "fidelity", "degradation_pattern": "Significant motion...", "ranking": { "xrestormer": 1, "mprnet": 2, ... }, "related_trajectory_ids": [0, 6, ...] }, { "exp_id": 1,...
D+M	Perception	{ "exp_id": 0, "degradation_type": "dark+motion blur", "preference": "perception", "degradation_pattern": "Significant loss...", "ranking": { "motion blur -> dark": 1, "dark -> motion blur": 2 }, "related_trajectory_ids": [0, 1, ...] }, { "exp_id": 1,...

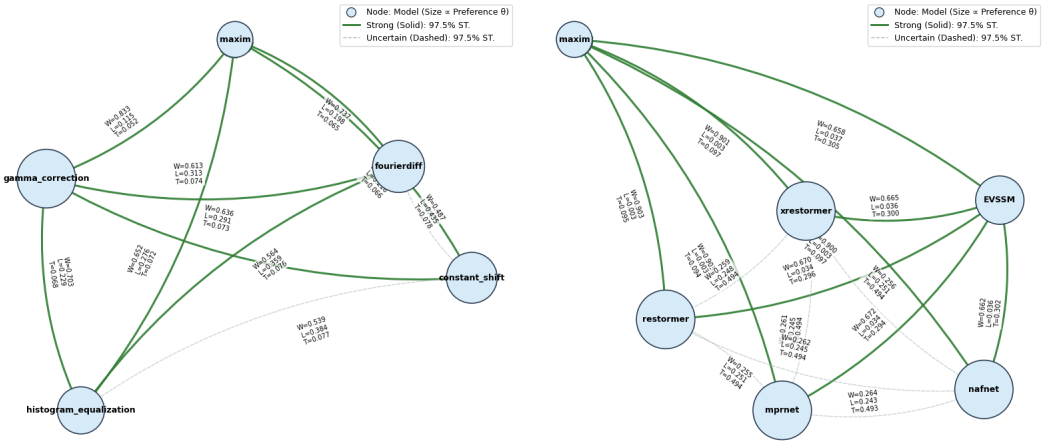

(a) BTD Complete Graph on 'Dark'

(b) BTD Complete Graph on 'Motion Blur'

Figure 12: Visualization of the BTD Model result in *Tool Selection*.

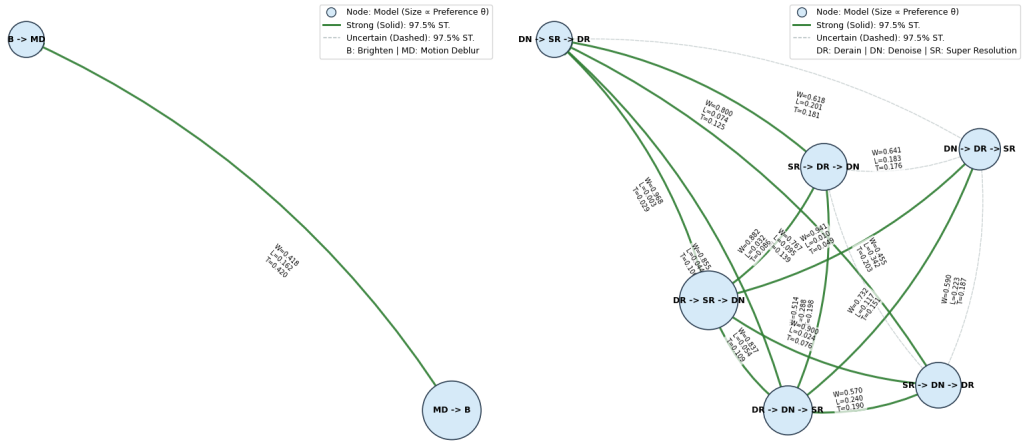

(a) BTD Complete Graph on 'Dark+Motion Blur' (b) BTD Complete Graph on 'Rain+Haze+LR'

Figure 13: Visualization of the BTD Model result in *Degradation Removal Order*.

B.5 Detail Ablation Study on Evolution Times

Table 9 and Figure 14 detail the ablation study of the self-evolving experience mechanism on GroupB of the MiO100 dataset with batch size $B = 25$. By systematically varying the number of evolution times, we seek to investigate the optimal balance point. We still utilize the *Unified Quality Index (UQI)* for performance measurement, while the *Total Rollback Times* for efficiency measurement.

Cost-Quality: As illustrated in (a), the system's evolution exhibits a convergent trajectory from the initial condition of Times $= 0$ to the condition of Times $= 2$. This trajectory is characterized by a steady increase in the UQI and a substantial decrease in the total rollback overhead. The system reaches the Pareto-optimal point at Times $= 2$ (top-left corner). However, for Times > 2, the curve folds back towards the bottom-right, indicating potential overfitting or experience redundancy. **Quality Progression:** The findings of in (b) indicate that the UQI exhibits a marked increase in growth during the initial phase (Times < 2) and attains its peak level of growth at the Times $= 2$ mark. The plateau and slight fluctuations show diminishing returns in the subsequent phase (Times > 2), suggesting that excessive evolution may hinder generalization. **Cost Breakdown:** Furthermore, the overhead breakdown in (c) explains that the substantial decrease in total rollback times (from 2.50 to 1.29) is predominantly driven by the reduction in T-Rb (Tool Execution Rollbacks), while O-Rb remains relatively slightly. This phenomenon demonstrates that our rollback strategy by fallback O first and then T, when combined with empirical information, can significantly improve efficiency, thereby providing a cost-effective path for reducing trial-and-error in the training-free IRA paradigm.

Overall, Times $= 2$ emerges as the optimal sweet spot between performance and efficiency. The self-evolving experience mechanism not only enhances the system's adaptation to the data source but also drastically reduces inference latency.

Table 9: Ablation study on evolving times with **EvoIR-Agent**. The best results are highlighted in **bold**. The derived metrics are highlighted with a shaded background.

Times	$B = 25$	Quality Metrics						Summary	Efficiency Metrics			Summary
		PSNR ↑	SSIM ↑	LPIPS ↓	MANIQA ↑	CLIP-IQA ↑	MUSIQ ↑	**UQI ↑**	Invoc. ↓	$\mathcal{O}$-Rb ↓	$\mathcal{T}$-Rb ↓	**Total Rb ↓**
0	0	20.59	0.6579	0.3287	0.2770	0.4603	56.69	0.06	5.41	0.67	1.83	2.50
1	25	22.21	0.7346	0.3430	0.3459	0.5091	61.26	0.57	4.16	0.63	1.04	1.67
2	50	**23.38**	0.7643	0.3117	0.3735	0.5296	61.96	0.93	**3.34**	**0.55**	**0.74**	**1.29**
3	75	23.03	0.7539	0.3205	**0.3749**	0.5180	**62.44**	0.85	3.74	0.60	0.91	1.51
4	100	23.04	**0.7647**	**0.3029**	0.3714	**0.5386**	61.79	**0.95**	3.99	0.71	0.94	1.65

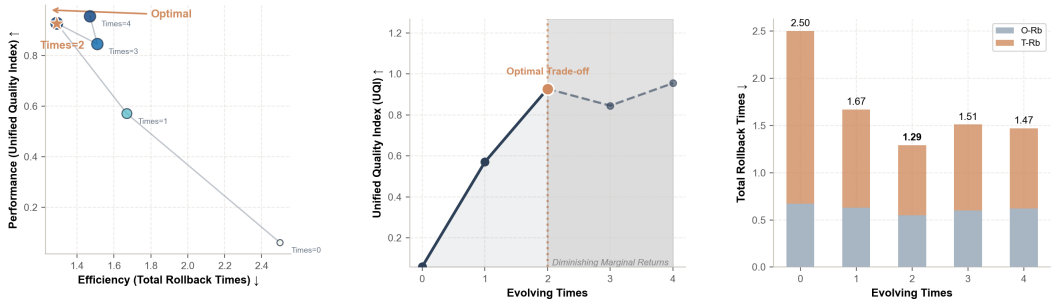

(a) Performance-Efficiency Trade-off.

(b) Quality Progression.

(c) Overhead Breakdown.

Figure 14: Performance-Efficiency analysis of the evolution process with batch size B=25. (a) Cost-quality Pareto front between performance (*Unified Quality Index*) and efficiency (*Total Rollback Times*). (b) Quality (Unified Quality Index) progression over evolution times, demonstrating clear diminishing marginal returns. (c) Decomposition of the total rollback times into O-Rb and T-Rb components during the evolving process.

B.6 More Qualitative Results

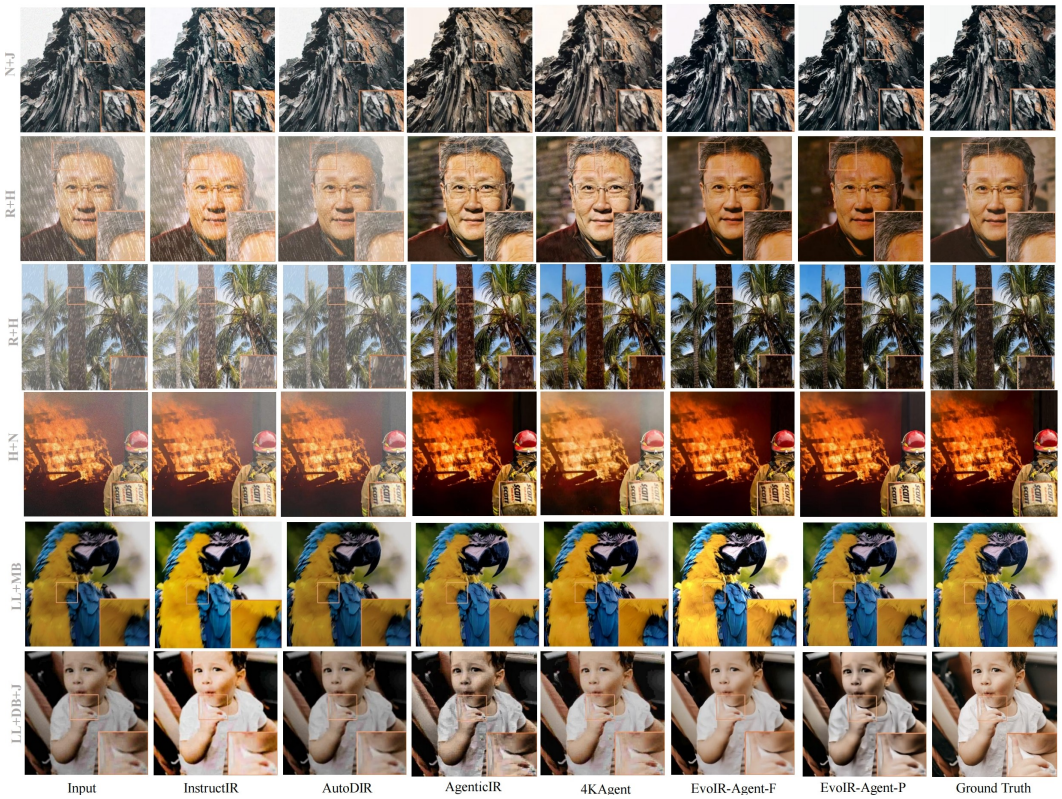

Figure 15: More visual comparison examples on MiO100 dataset. **EvoIR-Agent-F** denoted the fidelity *Preference* requirement, while **EvoIR-Agent-P** denoted the perception *Preference* requirement.

C Implementation Details

C.1 Tool Set

We leverage the methods in [16] during the *Perception* and *Reflection* processes. The entire experiment is conducted with two NVIDIA A6000 GPUs. Since the present framework is flexible to different tools, this property is examined in two tool sets. All the ablation studies are conducted on setting II with two *Preference* setting.

In the **EvoIR-Agent-I**, the configuration of the tool settings in previous agents [16, 19, 17] is adhered to.

- **Brightening:** CLAHE [60], Gamma correction ($\gamma = 2/3$), constant shift.
- **Defocus Deblurring:** DRBNet [61], IFAN [62], Restormer [63].
- **JPEG Artifact Removal:** SwinIR [64] (quality factor 40), FBCNN [65] (quality factors 90 and 5, and blind setting).
- **Denoising:** SwinIR [64], MAXIM [66], MPRNet [67], Restormer [63], X-Restormer [68].
- **Deraining:** MAXIM [66], MPRNet [67], Restormer [63], X-Restormer [68].
- **Motion Deblurring:** MAXIM [66], MPRNet [67], Restormer [63], X-Restormer [68].
- **Dehazing:** MAXIM [66], X-Restormer [68], RIDCP [69], DehazeFormer [70].
- **Super Resolution:** DiffBIR [71], HAT [72], SwinIR [64], X-Restormer [68].

In the **EvoIR-Agent-II**, the tool settings from prior agents [20, 18] are utilized.

- **Brightening:** CLAHE [60], Constant Shift (C=40), DiffPlugin [73], FourierDiff [74], Gamma Correction ($\gamma = 2/3$), MAXIM [66].
- **Defocus Deblurring:** ConvIR [75], DiffPlugin [73], DRBNet [61], IFAN [62], LaKDNet [76], Restormer [63].
- **JPEG Artifact Removal:** FBCNN [65] (QF=5), FBCNN [65] (QF=90), FBCNN [65] (BQF), SwinIR [64] (QF=40).
- **Denoising:** MAXIM [66], MPRNet [67], NAFNet [77], Restormer [63], X-Restormer [68], SwinIR [64].
- **Deraining:** DiffPlugin [73], MAXIM [66], MPRNet [67], Restormer [63], X-Restormer [68].
- **Dehazing:** DehazeFormer [70], DiffPlugin [73], MAXIM [66], RIDCP [69], X-Restormer [68].
- **Motion Deblurring:** EVSSM [78], LaKDNet [76], MAXIM [66], MPRNet [67], NAFNet [77], Restormer [63], X-Restormer [68].
- **Super Resolution:** DiffBIR [71], DRCT [79], HAT-L [72], HAT-GAN, HMA [80], OSEDiff [81], PiSA-SR [82], SwinIR [64], SwinIR (Real-ISR), SwinFIR [83], X-Restormer [68].

C.2 Experience Pool Setting

Implementation Details & Hyperparameters. Our framework is implemented with the following hyperparameter configurations:

- **Retrieval & Evolution:** The Top-K recall (Sec. 3.1) is set to 3. For experience evolution (Sec. 3.4), we set the trigger threshold batch size B to 25, the significance level α to 0.975, and the mini-batch size to 12.
- **IQA Metrics:** The metrics set for *Fidelity* consist of PSNR, SSIM, LPIPS, and DISTS. The *Perception* metrics set, utilized to support the *Preference* in Sec. 3.2, includes MANIQA, MUSIQ, BRISQE, CLIPIQA, NIQE, and NIMA.

MLLM Instantiation. The estimated API cost per round for the agent-driven pattern profile learning system is reported in Table 10.

- **Base Inference:** Qwen3-VL-Flash [84] is adopted for standard, general-purpose multimodal operations.
- **Experience Evolution:** To ensure deep image interpretation and high-quality description generation during fine-grained experience evolution, we employ the more capable Qwen3-Plus [84] foundation model.

Table 10: Detailed API usage and estimated cost for formulating fine-grained experience within a single mini-batch in **EvoIR-Agent**.

Model Name	Calls / Batch	Avg. Tokens / Call		Total Cost per Batch ($)
		Input	Output	
Qwen3-VL-Flash	∼35	∼950	∼150	0.0189
Qwen3-Plus	∼12	∼1,300	∼400	0.0931
Total	**47**	–		**0.1120**

C.3 Prompts

***Insight* Evolving Prompt**

```
Based on the following Bradley-Terry-Davison (BTD) probabilistic model
    results for multi-degradation image restoration tasks (Preference: {
    preference}), extracted key insights about the degradation removal order
    and recommendations:\n\n{combined_text}\n\n Your conclusion insight:
```

Multi-Agent Debate *Role* Prompt

```
Your role is to act as the {role}, the theme is: 'Is this a good enough
    degradation pattern?'. Which means you are good at dealing with
    information from yourself & other to think about the next appropriate
    action without executing it. Now is your thinking stage.

Historical information(your current stage reasoning & the external tools
    result): {context}.

You have access to external tools represented as Python function prototypes,
    which you may invoke to support your debate competition:
- generate_groups(no parameter)
- validate_current_group(traj_id: List[int]) # using to validate current
    unconvinced image degradation pattern(intra-group: within the same
    degradation pattern) by specified trajectories id(requirements: 1
    unconvinced traj_id + 1~3 convinced traj_id, totally 3 traj_id specified
    id is maximum)
- validate_other_group(traj_id: List[int]) # using to validate other
    unconvinced image degradation pattern(inter-group: between two
    degradation patterns) by specified trajectories id(requirements: 1
    unconvinced traj_id + 1~3 convinced traj_id, totally 3 traj_id specified
    id is maximum))
- finish(no parameter) # using when you think you have obtained the final
    answer

Your response must strictly follow this format. It's forbidden to include any
     output beyond these two sections:
Thought: [Your brief reasoning process must be less than 200 words, including
     problem analysis and analysis of the action to take on the next step.]
```

```
Action: [The ‘Python function prototypes‘ you decide to take on the next step
    .]:
```

Multi-Agent Debate *Action* Prompt

```
You want to ensure that all degradation patterns you raise are credible and
    accurate enough to withstand challenges in a debate competition. The
    theme is: ‘Is this a good enough degradation pattern?‘

Currently, there is an ongoing process defined as ’semantic clustering’.
The goal of semantic clustering is to categorize degradation modes.
The rules for semantic clustering are as follows:
1. Within each degradation pattern category, the semantic representation of
    the degradation pattern text information must be as similar as possible.
2. Between different degradation pattern categories, the semantic
    representation difference of the degradation pattern text information
    must be significant.
3. Under the premise of satisfying rules 1 and 2, the tool ranking
    information of the ‘top three(If only two, then top2)‘ within each
    degradation pattern category must be as close as possible.
4. Under the premise of satisfying rules 1 and 2, the tool ranking
    information of the ‘top three(If only two, then top2)‘ between different
    degradation pattern categories must be as distant as possible.
5. The number of degradation pattern categories is not fixed, but must avoid
    redundancy and dissatisfaction of the point mentioned in 1-4.
6. For uncertain trajectory information that cannot be confidently classified
     considering the semantic representation and ranking requirements,
    explicitly indicate which trajectories are uncertain and require further
    verification inside the XML label <unconvinced_info></unconvinced_info>
    or inside the <verify1></verify1>.

You are provided with the current degradation pattern categories derived
    solely from textual information: {pattern_textual_context}
Some categories contain trajectories with uncertain classification. Now, you
    will perform a further validation step using both the image information
    provided as: {pattern_image_context}

You can provide two types of judgments:
1. Positive: Confirm that the trajectory fits the degradation pattern
    category based on the image data.
2. Negative: Determine that the trajectory does not fit the current
    degradation pattern category; instead, select a more appropriate
    degradation pattern category based on textual semantic similarity and
    specify that cross-category verification is needed.

Finally, you need to keep the content inside <convinced_info></convinced_info
    > and (if they exist <unconvinced_info></unconvinced_info> <verify></
    verify> you need to keep them too) without removing any previous outputs
    and copy the previous output. For the current verification, should append
     behind that pattern inside the XML brace <verify_1></verify_1> with a
    number in sequence. Your output must strictly follow this format:
<convinced_info>Degradation Pattern 1: The pure semantic representation of
    the degradation pattern text information is..., included trajectories are
     Traj1, Traj3..., reasons are...,</convinced_info><unconvinced_info>among
     these trajectories, the classification of Traj1..., are not fully
    convincing because..., need further verification</unconvinced_info>.<
    verify_1>After combined text and image validation, Traj3 indeed belongs
    to Degradation Pattern 1, because...</verify_1>
```

Pattern Profile Operation *Function* Prompt

```
You are an expert in planning and knowledge management, tasked with updating
    degradation patterns stored within a vector database. Your objective is
    to analyze a given set of "new degradation patterns" alongside the "old
    degradation patterns" currently in the database, and determine the
    precise atomic operations required to keep the database accurate and up-
    to-date.
Specifically, for each new pattern, decide which of the following actions
    applies:

- add: Introduce a completely new pattern to the database because it does not
     overlap with existing ones. Using this operation to balance accuracy and
     redundancy.
- merge: Identify when an existing pattern fully subsumes a new pattern, in
    which case, retain the old pattern but enrich it with additional
    information from the new one.
- replace: Apply when the new pattern subsumes an existing pattern, meaning
    the new pattern's semantics are broader or more accurate, and thus should
     replace the old pattern.

You will receive a task description labeled that specifies the particular
    patterns to analyze. If you receive any feedback on your output, revise
    your operations accordingly while maintaining the same output format.
Current task description:
Degradation type: {degradation_type}
New degradation patterns: {new_pattern}

Existing degradation patterns in DB: {pattern_db}
Previous plans: {history_plan}
Previous feedback: {history_feedback}

Your output must be formatted as a Python list of strings, where each string
    represents a single atomic operation; it's forbidden to do an operation
    on the same old degradation pattern. If the operation is unsatisfactory
    on the degradation patterns, change to another degradation pattern.
The format for each element is:
"<new pattern digit only> | <action> | <existing pattern digit only(optional)
    >"
Include the existing pattern only when relevant (for merge or replace actions
    ). For add actions, the existing pattern field can be omitted.

Example output:
["1 | merge | 2", "2 | add"]
```

D Limitation and Future Work

While EvoIR-Agent establishes a robust and efficient training-free paradigm for an image restoration agent, there are still some boundaries that present exciting avenues for future research:

To guarantee the highest quality of atomic experience records, our current experience acquisition phase utilizes an exhaustive exploration strategy. While this approach maintains remarkable efficiency and optimal performance for typical coupled scenarios (e.g., 2 to 3 degradation types), scaling the system to highly entangled, extreme scenarios (e.g., 4 or more types) exponentially increases the combinatorial search space. Another boundary centered on the Pattern Profile Learning system for fine-grained experience modeling, which requires strong visual comprehension of the MLLM. Consequently, it currently relies on high-performance, state-of-the-art MLLMs. Utilizing lightweight or less capable models may occasionally introduce variances in output formatting or suboptimal semantic alignment, which can hinder the automated experience collection process.

Our future work is to integrate advanced exploration-exploitation balancing strategies into the experience acquisition process. This will ensure efficient experience formulation even under an expanding array of degradation types. To democratize the framework and eliminate reliance on massive, closed-source models, our future work will focus on experience distillation. We aim to finetune a domain-specific open-source MLLM dedicated to conclude experience in IRA, matching the reasoning accuracy of general large MLLMs while significantly reducing API costs.